Multi-proxy temperature and environmental reconstruction during the Late Glacial and Early Holocene in the Bohemian Forest, Central Europe

Amanda Mateo-Beneito a, Gabriela Florescu a b, Jolana Tátosová c, Vachel A. Carter a d, Richard Chiverrell e, Oliver Heiri f, Iuliana Vasiliev g, Niina Kuosmanen h i, Petr Kuneš a

Highlights

- Multi-proxy temperature reconstructions can overcome the limitations of the proxies and provide clearer climatic trends.
- Temperature reconstructions based on independent proxies used in our study follow a similar trajectory and high correlations.
- The cooling related to the onset of the YD was more marked during winter than summer, corroborating a higher seasonality.
- In the Bohemian Forest, the environmental response to the YD cooling was non-synchronous to other Western European records.

Abstract

Multi-proxy temperature reconstructions can provide robust insights into past environmental conditions. By combining different proxies we can disentangle the temperature signal from the indirect climate effects on the environment. This study uses a multi-proxy approach to reconstruct temperature and palaeoenvironmental conditions during the Late Glacial and Early Holocene (13.5–8 cal. ka BP) in the Bohemian Forest, Central Europe. We assessed the similarity of the temperature signal based on chironomids, isoprenoid glycerol dialkyl glycerol tetraether lipids (isoGDGTs), and pollen within a comparison with locally modeled temperature data generated by the CHELSA_Trace21k dataset. Pollen, macroscopic charcoal remains, and geochemistry were further used to reconstruct past environmental conditions such as vegetation dynamics, fire activity, the input of lithogenic material (Titanium), nutrient content (Total Nitrogen) and the sources of organic matter (C/N and δ13Corg). All temperature reconstructions based on independent proxies were positively correlated and followed the same long-term trend. However, results also showed that chironomids-inferred July temperature had lower amplitude variations compared to the other temperature curves. IsoGDGTs showed the most pronounced decrease in temperature values at the onset of the Younger Dryas (YD), corroborating that this cooling event was more marked during winter than summer. However, a decrease of less than 1 °C during summer and two short-term warm events at 12.6 and 12.2 cal ka BP provoked a modest and asynchronous response of the vegetation to the onset of the YD. Nevertheless, isoGDGTs appeared to react to changes in both temperature and organic carbon sources, particularly between 11.2 and 10.6 cal yr BP. These environmental changes, characterized by high values of the GDGT-0/crenarchaeol ratio, recorded an increase in methanogenic activity in the lake sediments, which likely altered the recorded climatic signal. The corresponding anoxic episodes in the lake sediments might be caused by an increasing input of organic carbon from the catchment, related to the development of the vegetation and catchment soils at the beginning of the Holocene. Finally, pollen-based temperature reconstruction showed a lag in the response to major climatic events, such as the onset of YD and Holocene. Our study increases the understanding of the climate-vegetation-environmental feedback during the Late Glacial and Early Holocene in the Bohemian Forest, Central Europe.

1. Introduction

The transition between the last glacial to the current interglacial period was marked by rapid and pronounced climatic oscillations that resulted in different climatic effects across the North Atlantic Region (Rasmussen et al.,

2006; Feurdean et al., 2014; Heiri et al., 2014; Moreno et al., 2014; Wohlfarth et al., 2018; Engels et al., 2022). For example, during the Late Glacial period (LG; 14.7 to 11.7 cal ka BP), the North Atlantic Region registered the most abrupt climatic shifts in Europe, as temperatures were noticeably influenced by the melting of ice sheets and changes in the North Atlantic thermohaline circulation (Clark et al., 2001; Renssen et al., 2015). The transition from the Allerød warm interstadial (All; 13.9–12.85 cal ka BP; Birks and Birks, 2014) to the Younger Dryas cold stadial (YD; 12.85–11.7 cal ka BP; Alley, 2000; Rasmussen et al., 2014), resulted in a decrease in summer temperatures of 4 °C in areas such as the Baltic region and the British Isles (Heiri et al., 2014). Meanwhile, territories in eastern and southeastern Europe, distant from the oceanic influence of the North Atlantic, experienced less pronounced temperature variations (Płóciennik et al., 2011; Tóth et al., 2012). Subsequently, for the Early Holocene (EH) (11.7–8 cal ka BP), the climatic conditions ameliorated, and a gradual temperature-increasing trend was established, interrupted by several short-term oscillations (Mayewski et al., 2004). However, how these large-scale abrupt climatic changes were recorded locally in Central Europe remains uncertain, due to the lack of climate reconstructions in this region.

The Bohemian Forest, located in a mid-latitude mountainous range in Central Europe between oceanic and continental climates, was occupied by local glaciers during the last glacial period. However, unlike other mountainous areas and northern latitudes, it did not experience glacier regrowth or expansion during the YD (Mentlík et al., 2013). While several paleoenvironmental reconstructions exist from the area, based on chironomids (Tátosová et al., 2006), cladocerans (Pražáková et al., 2006), pollen (Jankovská, 2006), plant macro remains (Vočadlová et al., 2015) and charcoal (Carter et al., 2018a), none of them provide a quantitative temperature record. Given that mountain regions are more sensitive to climate change (Birks and Ammann, 2000; Moser et al., 2019) and the Bohemian Forest is strategically placed at the transition between the oceanic and continental climates, it can offer a unique perspective on temperature changes during the LG and EH.

Lake sediments are excellent archives of past terrestrial and aquatic environments (Birks and Birks, 2006; Castañeda and Schouten, 2011). Proxies in lacustrine archives can be used to reconstruct temperature, each with its strengths and limitations. For example, subfossil chironomids (dipterans), whose larvae colonize different habitats including lake sediments, are a widely used paleo-temperature proxy due to the species specific sensitivity to July air temperature variations (Brooks, 2006; Eggermont and Heiri, 2012; Luoto and Ojala, 2017; Engels et al., 2020). However, chironomid assemblages can be affected by factors other than temperature, such as nutrient availability, lake depth or habitat disturbance (Heiri and Lotter, 2005; Brooks et al., 2007). Fossil pollen is mostly used for reconstructing past vegetation dynamics, but changes in pollen assemblages over time can also be used to reconstruct temperature patterns (Chevalier et al., 2020). Nevertheless, pollen-based temperature reconstructions have the disadvantage of assuming a constant relationship between pollen abundance and temperature and can be affected by species' migration lags, succession, and land use (Ortu et al., 2006). In addition to chironomids and pollen, membrane lipids produced by diverse species of Archaea, such as isoprenoid glycerol dialkyl glycerol tetraethers (isoGDGTs), can also provide temperature reconstructions. Specifically, the composition and structure of isoGDGTs within the Thaumarchaeota clade change in response to temperature (Schouten et al., 2013; Inglis and Tierney, 2020). The relative abundance of isoGDGTs has been linked to the annual surface temperatures of seas (Schouten et al., 2002; Kim et al., 2008) and lakes (Powers et al., 2010). However, the presence of other archaeal groups, such as Euryarchaeota which produce similar compounds but in a different distribution, can cause interference with the correlation between isoGDGTs and temperature. Unlike Thaumarchaeota, these groups respond to temperature and other environmental conditions in a different way, and their presence in lake sediments could affect the reconstructed climatic signal (Sinninghe Damsté et al., 2022). A multi-proxy temperature reconstruction has the potential to overcome the limitations of the individual proxies and reveal the main trends in temperature, especially during high-amplitude, abrupt climatic changes such as those pertaining to the last deglaciation (Birks and Birks, 2006), or point towards discrepancies between the different records. However, reconstructing past temperatures quantitatively is difficult due to the complex interactions within and between terrestrial and aquatic ecosystems. For example, in the case of chironomids and isoGDGTs, changes in lake productivity could impact the recorded temperature signal, as an increase in both productivity and temperature could cause oxygen depletion and an increase in nutrient supply to the lake system (Blaga et al., 2009; Sinninghe Damsté et al., 2012; Stivrins et al., 2021). Therefore, the environmental changes would impact the distribution of the species (chironomids) or compounds (isoGDGTs) in the lake sediments, thereby influencing the reconstructed temperature values, leading to a misinterpretation of the environmental changes as higher-amplitude climatic

fluctuations. Hence, reconstruction of local palaeoenvironmental conditions is a prerequisite for a reliable temperature reconstruction. Additionally, a combined approach of comparing proxy-derived paleo-temperature reconstructions with high-resolution downscaled global paleoclimate models would increase the robustness of the reconstruction and help inform how local-scale temperature changes relate to larger-scale climatic patterns.

Although multi-proxy studies are common nowadays, only a few have compared temperature reconstructions based on several different proxies from the same locality (Veski et al., 2015; Watson et al., 2018; Martin et al., 2020; Ramos-Román et al., 2022; Robles et al., 2023; d'Oliveira et al., 2023). This is likely because different proxies reflect the temperature signal of different seasons (e.g. annual, summer or winter) or habitats, such as lake surface, soils or air, complicating such comparisons. Thus, many studies that use multiple proxies tend to use proxies for the same season and habitat, which may not capture climatic variations that occur outside of the recorded seasons. For example, in the Southern Carpathians, Tóth et al. (2012) detected no cooling related to the YD during summer inferred by chironomids, while Buczkó et al. (2012) found a longer ice cover period at the same lake based on diatoms. Moreover, Veski et al. (2015) compared summer and winter temperatures during the LG and EH in the Baltic-Belarus area and found that reconstructed temperature values decrease less in summer than in winter. It has been suggested that the YD was a period of high seasonality, with an abrupt decrease in winter temperatures but relatively warm and short summers (Birks and Birks, 2014; Tóth et al., 2012; Heiri et al., 2014; Müller et al., 2021). However, there are currently no studies in Central Europe that compare proxies that reflect temperature changes in different seasons to explore this possibility.

This study provides the first quantitative mean annual and mean July temperature reconstructions during the LG and EH (13.5–8 cal. ka BP), as well as the first comparison of proxy-derived palaeo-temperature reconstructions with local palaeoenvironmental change and modeled palaeotemperature from the Bohemian Forest. The abrupt climatic oscillations that occurred during the LG and the onset of the Holocene warming provide an opportunity to evaluate how the different proxies used in this study respond to abrupt temperature changes in this region. The main aims of this study are to (1) reconstruct the LG and EH temperatures using three different proxies (chironomids, isoprenoid GDGTs and pollen) and compare their responses with local temperatures inferred from a downscaled climate model; and 2) reconstruct the environmental response of the lake ecosystem and assess its potential influences on the reconstructed temperature signal.

2. Material and methods

2.1. Study area

The lake Černé jezero (49°10’45.0 ”N 13°10’57.0 ”E) is located in the Bohemian Forest, Czech Republic (Fig. 1A), at an elevation of 1008 m.a.s.l. It has an area of 18.8 ha and a catchment area of 128 ha (Janský et al., 2005). The lake is of glacial origin, with the glaciers melting approximately 14 cal. ka BP (Mentlík et al., 2013). The lake has two basins, the larger one with a maximum depth of 40.1 m close to a steep lake wall, and the smaller one with a depth of 17 m (Janský et al., 2005). The bedrock is formed by metamorphic mica schist with intercalations of quartzite (Kopáček et al., 2001). Local soils are thin rocky cambisols and podzols poor in nutrients. Similar to other glacial lakes in the Bohemian Forest, Černé jezero was affected by modern acidic deposition. Its biological recovery (modern pH 5) is delayed because of the lack of carbonates in the bedrock and soils, which affects its buffering system (Kopáček et al., 2016; Čtvrtlíková et al., 2023). The lake is oligotrophic, dimictic with mixing periods in spring and autumn and no anoxia at the bottom during the stratification periods (Kopáček et al., 2001). Nine inflows feed the lake, of which two are permanent (Fig. 1B), and the lake has only one artificial surface outflow, which has been used for a small hydroelectric power station since the 1920s. The modern lake level varies ∼1 m per year due to evaporation, outflow and the use of water for the hydroelectric power station. However, the water balance remains stable (Kopáček et al., 2001).

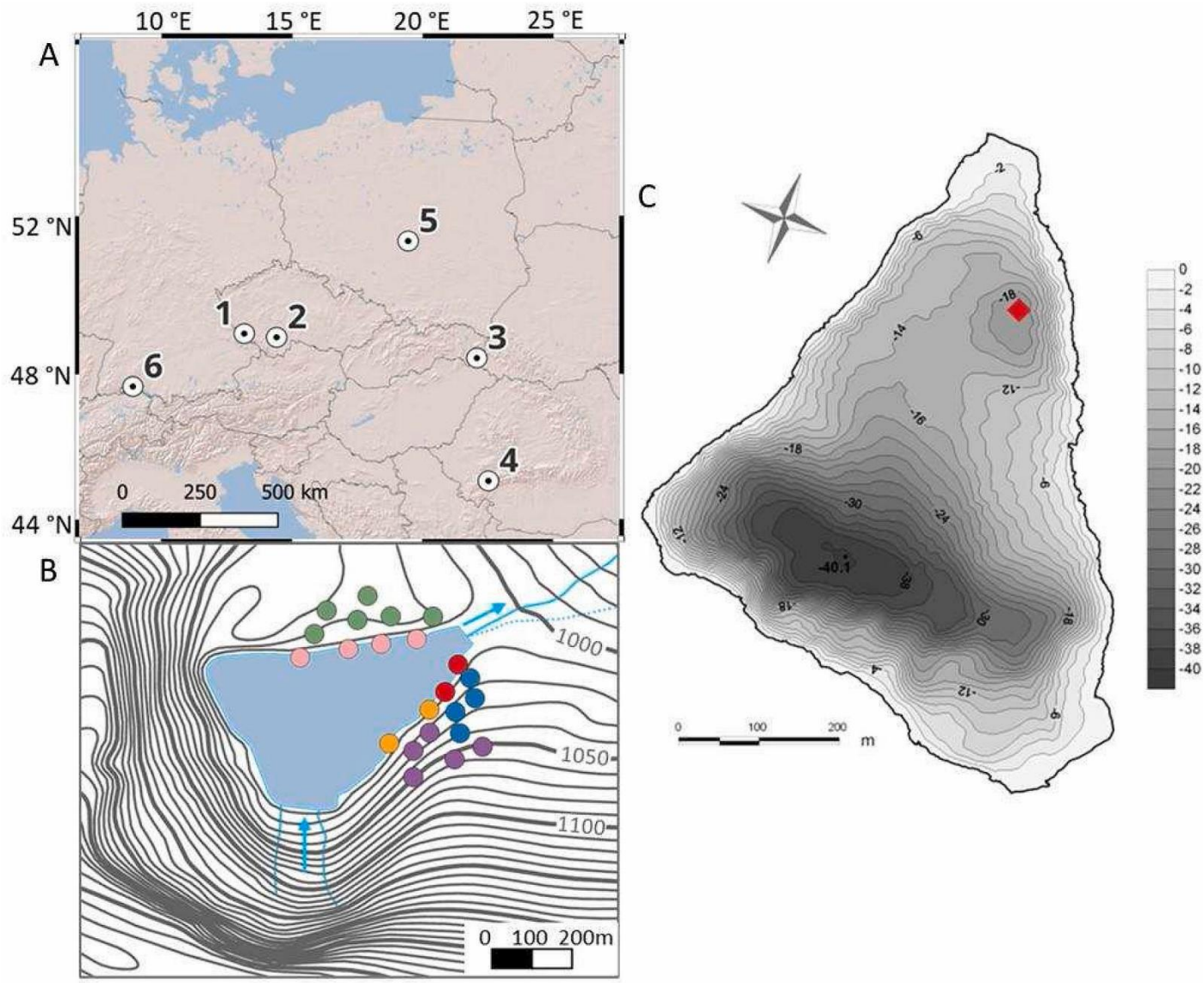

Fig. 1. Map of the study region. (A) Location of the study site (1 = Černé jezero, Czech Republic) in relation to regional sites used for comparisons from Central-Eastern Europe: 2 = Švarcenberk, Czech Republic (Kubovčík et al., 2021; Pokorný, 2002); 3 = Hypkaňa, Slovakia (Hájková et al., 2016); 4 = Lake Brazi, Romania (Buczkó et al., 2012; Tóth et al., 2012); 5 = Żabieniec, Poland (Płóciennik et al., 2011; Kotrys et al., 2020); 6 = Steiβlinger See, Germany (Schwark et al., 2002). (B) Topographic map of the lake catchment; the dots represent soil sampling points, color-coded to show how the subsamples were merged (green, purple, and blue represent forest soil samples, while pink, orange and red are lakeshore samples). The blue arrows represent the permanent inflows and outflow of the lake. (C) Bathymetric map of Černé jezero from Janský et al. (2005); the red dot marks the coring location.

Catchment vegetation is mainly composed of Norway spruce (Picea abies), with a minor presence of European beech (Fagus sylvatica), silver fir (Abies alba), rowan (Sorbus aucuparia), and sycamore (Acer pseudoplatanus). Understory vegetation is dominated by grasses such as Calamagrostis (Čížková et al., 2011). The climate of the area is temperate, with wet and cold winters and wet and mild summers. The mean annual temperature for the catchment of Černé jezero is 4.1 °C, mean July temperature is 12.9 °C, and mean January temperature is −4.5 °C (Turek et al., 2014). The average annual rainfall is 1432 mm year−1, and the ice cover generally persists from December to April (1960–1990) (Turek et al., 2014; Kopáček et al., 2001).

2.2. Core sampling and chronology

A sediment core was taken in August 2015 in the shallower basin at 17.05 m water depth (Fig. 1C). One gravity core and three drives of 1.5 m in length were recovered from a floating platform using a 1.5 × 0.075 m dimension Russian corer. An absolute depth of ~4 m of lake sediment was recovered until reaching the bedrock at 21.02 m from the lake water surface. The second and third recovered drives overlapped by 50 cm. In this study, we present the results from

the second drive, with depths expressed in centimeters below the lake water surface (cm b.l.w.s.) (1888–1998.5 cm b.l.w.s.).

Seventeen samples consisting of bulk sediment and selected macro remains from the first two drives (Table 1) were dated by Accelerator Mass Spectrometry (AMS). Measurements were performed at the Poznán Radiocarbon Laboratory, Poland, at the Center for Applied Isotope Studies (CAIS), University of Georgia, USA, and at the Isotoptech Laboratory in Debrecen, Hungary. The upper-most part of the first drive was dated using a Pb-210 radionuclide dating series based on eleven samples. The IntCal20 curve (Reimer et al., 2020) was used for calculating the calibrated years from the 14C ages (Fig. 2), integrating the data with the Bayesian method "BACON" (Blaauw and Christen, 2011). The Bayesian analysis partitioned the core into sixty 5 cm sections estimating the accumulation rate for each section by the MCMC approach, constrained by prior information on accumulation rate (gamma distribution of 50 cm per year and shape 2) and its variability as memory (a beta distribution with mean 0.4 and strength 24).

Laboratory ID	Depth (cm b.l.w.s.)	Dating method	^{14}C Age	Calibrated yr BP	Material
UGAMS-35703	1731.25	AMS	910 ± 25	730–905	needles
Poz-92325	1761.25	AMS	1915 ± 30	1725–1957	bulk gyttja
UGAMS-35704	1800.25	AMS	3040 ± 20	3143–3350	needles
DeA-26056	1831	AMS	4197 ± 35	4586–5052	bulk
Poz-92326	1851.25	AMS	5370 ± 40	5933–6202	needles
DeA-34989	1871.5	AMS	5733 ± 27	6466–6689	bulk
UGAMS-35705	1880.75	AMS	6000 ± 25	6824–7218	bark
DeA-34991	1882	AMS	6511 ± 34	6922–7392	bulk
DeA-26058	1896	AMS	7511 ± 38	8187–8400	bulk
DeA-26060	1903.5	AMS	7931 ± 42	8179–8416	bulk
Poz-92327	1910.25	AMS	8410 ± 50	9091–9483	bulk
UGAMS-38338	1918.5	AMS	8590 ± 20	9718–9548	spruce needles
DeA-26062	1934.5	AMS	9312 ± 40	10286–10651	bulk
Poz-80180	1949.75	AMS	9810 ± 10	11184–11290	bulk gyttja
UGAMS-35701	1963.75	AMS	10 460 ± 30	11832–12286	pollen concentrate
UGAMS-30706	1976.25	AMS	10 190 ± 30	12313–12580	pollen concentrate
UGAMS-35702	1980.75	AMS	10 610 ± 30	12494–12703	pollen concentrate

Table 1. Radiocarbon dating results for the Černé jezero first two drives that were used to construct the age-depth model.

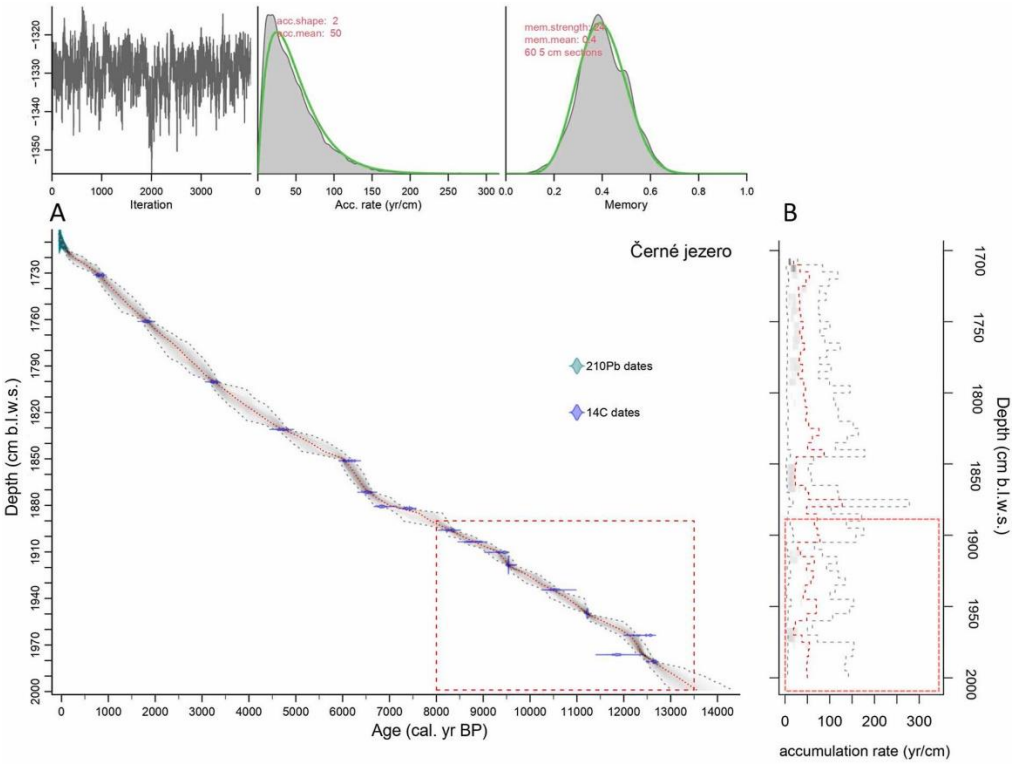

Fig. 2. A) Age-depth model based on Bayesian integration of the data, following the modeling routine 'BACON'. The red box indicates the section of sediment used for this study. B) Mean accumulation rates for the sediment core indicated by the red line. Grey lines represent the minimum and maximum accumulation rates. The red box indicates the studied period.

2.3. Chironomid analysis

A total of 42 chironomid samples were analyzed with downcore resolutions ranging from 0.5 to 12 cm. The amount of sediment processed per sample ranged from 0.8 to 2.2 g of dry weight, depending on the organic composition of each sample. The sediment samples were deflocculated in a 10% KOH solution for 40 min, stirred at 120 rpm at 60 °C, and then passed through an 86 µm sieve (Brooks, 1997; Walker et al., 1991). Head capsules were picked under a stereomicroscope at 45× magnification and mounted on slides in an Euparal mounting medium. When counting, head capsules that have half of the mentum were considered as a single individual. Head capsules were identified to species or genus level following Brooks et al. (2007) and Rieradevall and Brooks (2001) using a 400× magnification. Of the total 42 samples, nine samples from the LG did not reach the required minimum of 50 head capsules needed to reconstruct July air temperatures (Heiri and Lotter, 2001). Hence, they were merged with neighbouring samples, leaving a total of 35 samples used to create the temperature reconstruction. Concentration estimates were standardized to the number of head capsules per 1 g of dry sediment.

Chironomid-inferred mean July air temperature was reconstructed using the Swiss-Norwegian modern calibration dataset (Heiri et al., 2011), applying a Weighted Average-Partial Least Square regression model (WA-PLS) (ter Braak and Juggins, 1993). The root-mean-square error of prediction (RMSEP) of the applied temperature inference model is 1.38 °C and an R2 of 0.91 when the performance was tested within the Swiss-Norwegian calibration dataset using bootstrapping. The optimal splitting by information content method was used for differentiating the distinct stratigraphic zones regarding the chironomid species assemblage using the program Psimpoll (Bennett, 1993), and the number of significant zones was assessed by the broken stick model (Bennett, 1996) performed using R software (RStudio version 4.2.2; R Development Core, 2021). All the presented proxies follow the zonation marked by the chironomid data. The chironomid diagram was produced using 'Tilia' v.3.0.1 (Grimm, 1991).

2.4. Pollen

For pollen analysis, 69 subsamples of 0.5 cm3 were extracted every 2 cm and were processed using the standard method developed by Faegri and Iversen (1989), which involved the removal of the mineral fraction by HF and HCl followed by acetolysis. A known amount of Lycopodium spores was added to the samples prior to the sample preparation to calculate pollen concentration (Stockmarr, 1971). Residues were then mounted in glycerol and the

pollen grains and spores were identified and counted under a stereomicroscope at 400× magnification using Beug (2004), Punt et al. (1976) and the pollen reference collection at Charles University in Prague. Pollen concentrations were converted to accumulation rates (influx) using the sample ages from the Bayesian age-depth model. The influx pollen diagram was constructed in 'Tilia' v.3.0.1 (Grimm, 1991).

The pollen-based mean annual temperature reconstruction was done using modern pollen and climatic data procured from the Eurasian Modern Pollen Database 2 (EMPD2) (Davis et al., 2020). Only a subset of sites (north of 39°N latitude and between longitudes of 0° and 90°E) covering a substantial climatic gradient for our site while respecting biogeographical limits was used for model calculations (Fig. S1). First, we applied three different pollen-based methods −WA-PLS, MAT, and Random Forest (RF)−, of which RF was selected for further evaluation (see Supplementary Text for details). The model regression was carried out in R package "randomForest" (Liaw and Wiener, 2002) with n = 500 trees and the number of taxa divided by 3 at each split. The root mean square error of prediction based on the out-of-bag testing dataset is reported as sample-specific temperature prediction errors.

2.5. Charcoal

Macroscopic charcoal was used as a proxy for past changes in local fire history (Whitlock and Larsen, 2001). Macro-charcoal was sampled continuously at 1 cm resolution along the core. Subsamples of 1.5 cm3 were pretreated overnight with a solution of potassium hydroxide (KOH, 5%) to deflocculate clay particles, and a solution of sodium hypochlorite (NaOCl, 2%) to bleach non-charred organic matter. Samples were wet-sieved through a 125 µm mesh and all charred particles larger than 125 µm were counted under a stereomicroscope. Macroscopic charcoal counts were transformed to concentrations (# cm3) and then to accumulation rates based on the sediment deposition time extracted from the age-depth model.

2.6. GDGTs

To measure the GDGT content, 36 samples of ∼4 g wet lake sediment (with a resolution of 1–8 cm) were analyzed. Additionally, in 2020 six surface soil samples were collected from the catchment soils at a depth of 0–5 cm in the soil layer. Each sample represented a pooled composite of 3–6 subsamples taken in transects from the forested part to the lakeshore (Fig. 1B). All samples (modern and fossil GDGTs) were analyzed following the same methodology. Samples were freeze-dried, homogenized in an agate mortar, and extracted using a solution of dichloromethane and methanol (DCM: MeOH; 9:1; v:v) in a Büchi Speed Extractor for pressure-assisted solvent extraction. Total lipid extracts (TLE) were dissolved in DCM and desulphurized overnight on a magnetic stirrer, using copper turnings previously activated in a 10% HCl solution. TLE were further filtered through a combusted Na2SO4 plugged glass pipette. Columns with activated Al2O3 as a stationary phase were prepared to separate TLE into apolar, ketones and polar fractions. The column was washed with hexane: DCM (9:1; v:v) solution to separate the apolar fraction containing n-alkanes, then with DCM to remove ketones, and finally with DCM: MeOH (1:1; v:v) to obtain the polar fraction which contains the GDGTs (Butiseacă et al., 2022). The polar fraction was further concentrated to 2 mg/ml, then dissolved in 1 ml of hexane: isopropanol (99:1; v:v) mixture and filtered using a 0.45 µm PTFE filter. GDGT lipids were determined using a Shimadzu, Ultra-Fast Liquid Chromatography (UFLC) performance high-performance liquid chromatography coupled with an ABSciex 3200 QTrap chemical ionization mass spectrometer (HPLC/APCIeMS). The separation was achieved on an Alltech Prevail© Cyano 3 mm, 150−2.1 mm analytical column fitted with a 2.1 × 5 mm pre-column of the same material and maintained at 30 °C (after Hopmans et al., 2016). GDGTs were eluted isocratically using hexane, followed by hexane: isopropanol (9:1). Both isoprenoidal and branched GDGTs were analyzed via single acquisition for each sample. Detection was achieved through single ion monitoring (scanned masses: 1302, 1300, 1298, 1296, 1292, 1050, 1048, 1046, 1036, 1034, 1032, 1022, 1020 and 1018). Peak integration was done manually using the Analyst software v. 1.5.1 and referenced to an inhouse standard while peaks were integrated manually for each sample two times. All these analyses were performed at the Biomarkers Laboratory of the Senckenberg BiK–F in Frankfurt am Main, Germany.

The TEX86 index for the mean annual lake surface temperature (ALST) reconstruction was calculated following Schouten et al. (2002). To reconstruct the temperature, we used a calibration set that exclusively relied on isoGDGTs found in worldwide lacustrine sediments (Powers et al., 2010). Among the different calibration functions presented in the paper - annual, summer, and winter - we chose the one for mean annual temperature because it had an R2 = 0.88 and an RMSEP of 3.6 °C.

(1)TEX86 = (GDGT-2 + GDGT-3 + cren') / (GDGT-1 + GDGT-2 + GDGT-3 + cren')

(2)ALST = −14.0 + 55.2 * TEX86

The GDGT-0/cren ratio and the percent contribution of GDGT-2 to the sum of GDGT-1, -2, -3 and cren' (%GDGT-2) were also calculated to assess the contribution to the GDGT lipid pool of methanogenic archaea (which synthesize GDGT-0 and GDGT-1 to -3) and Thaumarchaeota archaea (which synthesised GDGT-1 to -3, crenarchaeol and the crenarchaeol isomer) in the recorded climatic signal (Sinninghe Damsté et al., 2012).

(3)%GDGT-2 = (GDGT-2 / (GDGT-1 + GDGT-2 + GDGT-3 + cren')) * 100

We calculated the branched to isoprenoidal tetraether (BIT) index (Hopmans et al., 2004), the MBT' and CBT indices to determine the relationships of brGDGTs with temperature and pH (Weijers et al., 2007; Peterse et al., 2012), and the brGDGTs IIIa/IIa ratio to address the source of brGDGTs into the lake sediments (Xiao et al., 2016; Martin et al., 2019).

(4)BIT = (Ia + IIa + IIIa) / (Ia + IIa + IIIa + cren)

(5)MBT' = (Ia + Ib + Ic) / (Ia + Ib + Ic + IIa + IIb + IIc + IIIa)

(6)CBT = -log (Ib + IIb) / (Ia + IIa)

2.7. Geochemistry and isotopic analysis (C and N)

The cores were cleaned and photographed at 15 µm resolution using the Line-scan camera fitted to the University of Liverpool Geotek Multi-sensor Core Logger (MSCL), then covered with 5 µm polypropylene film. Element geochemistry was measured by X-ray fluorescence (XRF) at 5 mm intervals on a wet sediment basis using the Olympus Delta energy dispersive µXRF mounted on the Liverpool Geotek MSCL (Boyle et al., 2015; Schillereff et al., 2015). The Olympus XRF undergoes daily laboratory consistency checks and regular measurement of certified reference materials (see Boyle et al., 2015). Titanium counts (Ti) were used as an indicator for the input of lithogenic material resulting from the physical erosion of the catchment bedrock (Hošek et al., 2017). The ratio between silica (Si) and titanium (Ti) was used as a qualitative proxy for biogenic silica (e.g. diatoms) (Brown, 2015).

δ13Corg isotopic composition, total carbon and total nitrogen content were measured on 54 samples. We used the C/N ratio and δ13Corg to trace the origin of sedimentary organic matter (allochthonous vs. autochthonous) (Meyers, 1994; Meyers and Lallier-Vergès, 1999; Teranes and Bernasconi, 2005). The samples were dried at 50 °C for 24 h, homogenized using an agate mortar, weighted, and wrapped into tin capsules. The measurements were conducted in the Stable and Radiogenic Isotope Research Centre of Charles University in Prague. The samples were combusted using a Thermo Flash 2000 elemental analyzer connected to a Thermo Delta V Advantage isotope ratio mass spectrometer (MS) in a Continuous Flow IV system. Released gasses were separated in a gas column (GC) chromatography and transferred to an MS to analyze the stable isotopic composition. Isotope ratios are reported as delta (δ) values and expressed relative to VPDB for δ13Corg, delta values were normalized to a calibration curve based on international standards. As the bedrock contained no carbonates, it was assumed that the amount of organic carbon (TOC) was equal to the total carbon (TC). The data were plotted using the C2 program (Juggins, 2003).

2.8. Local modeled temperature

To compare with the proxy data, we used a modeled long-term time series for the mean annual temperature (CHELSA-MAT) and the mean temperature of the warmest quarter (CHELSA-ST), extracted from the CHELSA_TraCE21k database. All data were cropped to a 1 km grid around Černé jezero, which had an average altitude of 1016 m a.s.l. The CHELSA climatic model incorporates the reconstructed paleo orography and provides temperature estimates since the Last Glacial Maximum at 100-year intervals (Karger et al., 2023). The spatial resolution of the model is 1 km2, which assures a better representation of the local climatic signal. As CHELSA is an algorithm based on a General Circulation Model, it may exhibit differences in modeled vs. real temperature values (Maraun, 2016). We quantified this error by subtracting modern observed temperature (1960–1990) from the simulated temperature values for the selected grid (Karger et al., 2023), which resulted in a discrepancy of 3.1 °C.

2.9. Statistical analysis

To compare the reconstructed and modeled temperature series, we detrended and calculated Pearson correlation coefficients. We also performed an unconstrained analysis of the detrended and normalized temperature series using a Principal Component Analysis (PCA). All the statistical analyses were done using R (RStudio version 4.2.2; R Core

Team, 2022) and the "vegan" package (Oksanen et al., 2022), after interpolating the data to the sampling resolution of the proxy with the lowest time resolution (isoGDGTs).

3. Results

3.1. Chronology and sedimentation rates

The age-depth model shows that the sedimentary sequence was deposited between 13.5 cal ka BP and the present (Fig. 2A). The time interval covered in this study (13.5–8 cal. Ka BP), showed no signs of a hiatus. The oldest dated sample corresponds to the depth of 1980 cm b.l.w.s. (12.5–12.7 cal ka BP; Table 1), so uncertainties could be higher in our age estimates before this period. The accumulation rate during the studied period varies between 22 and 79 yr/cm (average 51 ± 14; Fig. 2B), showing the lowest values (<30 cm/yr) between 1975 and 1965 cm b.l.w.s. (12.4–12.2 cal ka BP) and the highest (>70 cm/yr) between 1901 and 1905 cm b.l.w.s. (8.9–8.6 cal ka BP).

3.2. Chironomid record

Based on the broken stick method (Bennett, 1996), zonation of the chironomid taxa (Fig. 3) resulted in three significant zones. However, the analysis also showed a non-significant partition of the second zone into two, considered in this study as two subzones.

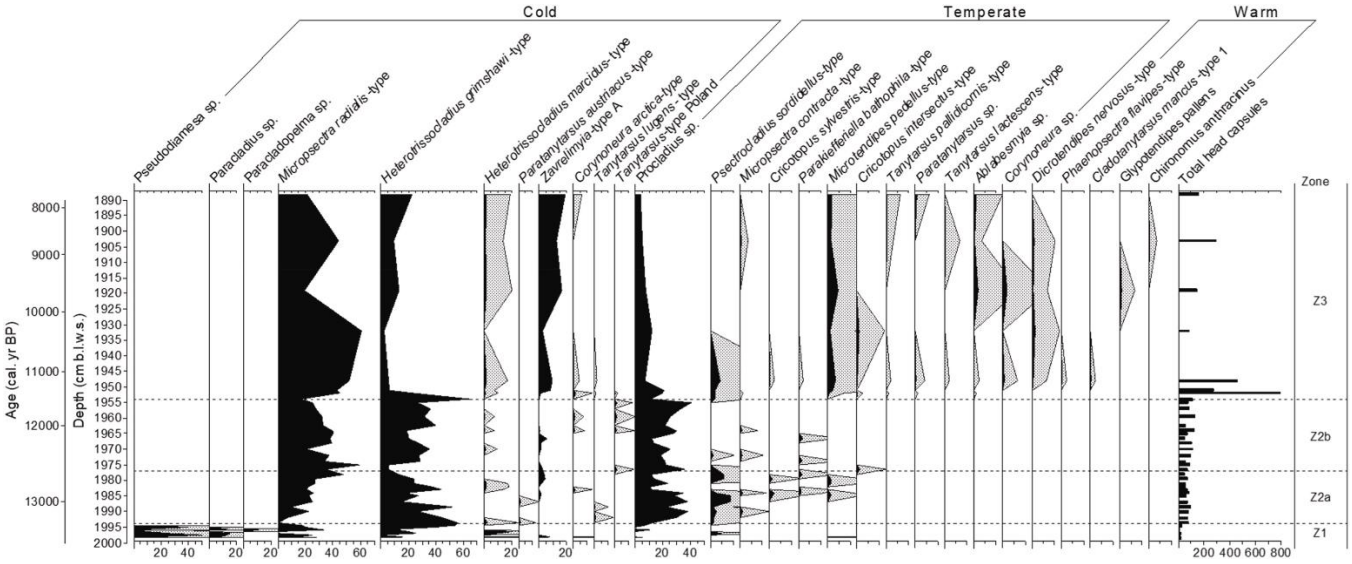

Fig. 3. Stratigraphic diagram showing the most important chironomid taxa. The x-axis shows percentage data of the total head capsules, except the sum expressed as the total amount of head capsules counted in each layer.

Zone 1 (Z1; 13.5 to 13.35 cal ka BP) was characterized by the presence of oligotrophic and ultraoligotrophic, cold stenotherm taxa such as Pseudodiamesa sp., Paracladius sp., and Paracladopelma sp., which were found only in this zone. Other cold-demanding taxa, such as Micropsectra radialis-type and Heterotrissocladius grimshawi-type, were also present (19% and 18% respectively). Taxa with a wider temperature range of tolerance, such as Procladius and Zavrelimyia, were found in lower numbers (2%). This zone was characterized by a low abundance of head capsules.

In Zone 2a (Z2a; 13.35 to 12.5 cal ka BP), M. radialis-type and H. grimshawi-type dominated the community (21% and 33% respectively). M. radialis-type decreased while H.grimshawi-type increased, indicating temperature amelioration. Even if H.grimshawi-type is still a cold-adapted taxon, its temperature optimum is wider than M.radialis-type (Heiri and Lotter, 2010). Taxa with a broader thermal tolerance, such as Paratanytarsus austriacus-type, Tanytarsus lugens-type, and Psectrocladius sordidellus-type are also found. Additionally, we identified chironomids often associated with macrophytes (i.e., Psectrocladius sordidellus-type, Parakiefferiella, or Microtendipes pedellus-type), and an increase in predators, such as Procladius.

In Zone 2b (Z2b; 12.5 to 11.5 cal ka BP), the cold and oligotrophic taxa, M.radialis-type (34%) and H.grimshawi-type (28%) remained dominant. Temperate and littoral taxa such as M.pedellus-type decreased, while Corynoneura arctica-type and Tanytarsus-type Poland appeared for the first time.

In Zone 3 (Z3 11.5 to 8 cal. ka BP), although the cold-demanding taxa, M.radialis-type and H.grimshawi-type, still dominated, the community diversified with the first arrival of warm-indicating taxa such as Ablabesmyia,

Dicrotendipes nervosus-type, Phaenopsectra flavipes-type, Cladotanytarsus mancus-type, and Glypotendipes pallens-type. The temperate M.pedellus-type and P.sordidellus-type reappeared. The highest density of head capsules in the whole record was found at the beginning of this zone.

3.3. Pollen record

Zone Z1 (13.5–13.35 cal ka BP) had the lowest pollen accumulation rate (PAR) of the entire record (Fig. 4), mainly comprised of herbaceous plants such as Helianthemum nummularium-type, Dryas octopetala, and Thalictrum, typical of open habitats and cold conditions. Wet-indicative taxa like Urtica and Cyperaceae were also found in Z1, as were shrubs such as Juniperus, Salix and Betula nana. In addition, pollen from forest-forming taxa, such as Quercus, Alnus, and Picea abies was also present with the lowest values of the record.

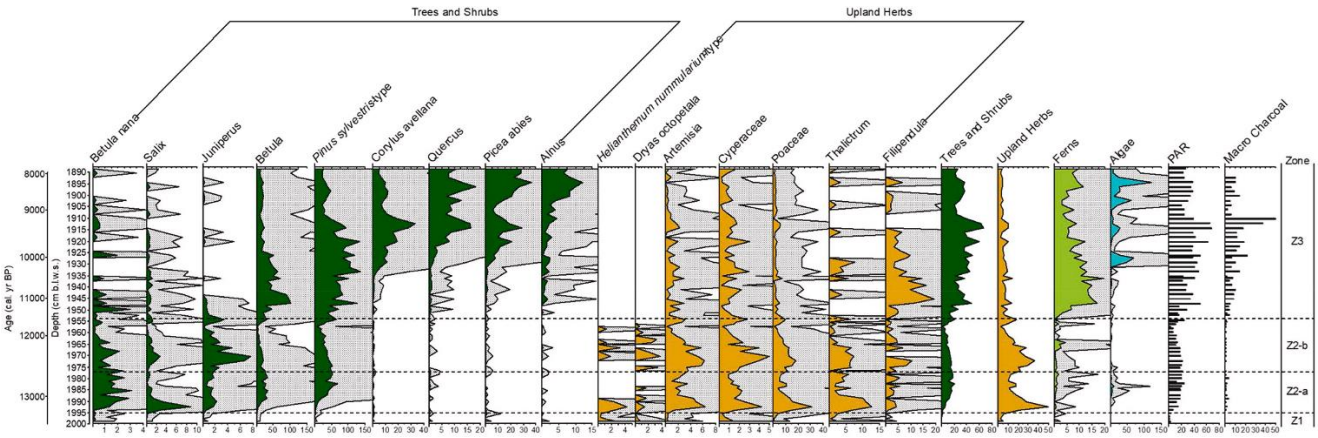

Fig. 4. Stratigraphic diagram of selected pollen taxa, expressed by pollen influx. The accumulation rates of macro charcoal remains are also plotted (# cm-2 yr-1). All taxa on the x-axis are scaled down by a factor of 100 for visual reasons, except for Trees and Shrubs, Corylus avellana and PAR groups (scaled down by 500) and Helianthemum nummularium-type, Dryas octopetala, Thalictrum and Filipendula (scaled down by 10).

During Zone Z2a (13.35–12.5 cal ka BP), PAR increased slightly while non-arboreal pollen (NAP) reached peak values. Taxa such as Artemisia, Cyperaceae, Helianthemum nummularium-type, and Thalictrum dominated at the beginning of this zone, accounting for 70% of the total PAR. However, these taxa were outcompeted by shrubs (i.e., Salix, Juniperus, and Betula nana) and trees, such as Betula and Pinus sylvestris-type, composing a mixture of shrub tundra and steppe patches with some dispersed trees which remained stable during the second half of Z2a. Ferns (Polypodiophyta) and algae (Botryococcus braunii) both increased at the end of this zone.

Zone Z2b (12.5–11.5 cal ka BP) is characterized by cold-tolerant taxa, with the highest PAR of Dryas octopetala occurring in this zone (Fig. 4). Other herbaceous taxa, such as Poaceae, Artemisia, Cyperaceae, and Thalictrum, also increased along with cold-tolerant shrubs like Salix and Juniperus. Trees such as Betula and Pinus sylvestris-type were still present but at similar or slightly decreasing values compared to Z2a.

Zone 3 (11.5–8 cal. ka BP) is defined by the highest PAR of the entire record (Fig. 4). Herbaceous light-demanding taxa, like Helianthemum nummularium-type, disappeared. Betula and Pinus sylvestris-type increased to their highest PAR values at 11 cal. ka BP. Pollen of mesophilic species increased, such as Corylus avellana, Picea abies, and Quercus, indicating the beginning of a mixed deciduous forest, with a peak in PAR at 9.4 cal ka BP. Ferns increased at the beginning of this zone, and algae taxa (Botryococcus braunii) increased at 10.5 cal ka BP, showing increasing biological activity first in terrestrial and later in the aquatic ecosystems.

3.4. Charcoal

Macro charcoal remains were scarce in Z1, Z2a and Z2b, indicating a low fire activity during the LG in our study area (Fig. 4), probably because of the lack of biomass as a combustible. However, macro charcoal influx slightly increased in Z2a compared to Z1 and Z2b. Fire activity increased at the onset of the Holocene (Z3), following a similar pattern as the total increase in PAR and trees and shrubs. The highest peak in macro charcoal occurred at 9.4 cal ka BP, followed by a sudden decrease.

3.5. GDGTs

We show the relative abundances of both isoprenoid and branched GDGTs from the lake sediments of the studied period and the modern soils (Fig. 5, Fig. S4). Among the isoGDGTs from the lake sediments, GDGT-0 is the most abundant in all the samples, followed by crenarchaeol (except in the last two samples at 7.8 and 8.1 cal ka BP where crenarchaeol is the most abundant compound). There are no GDGTs data for Z1.

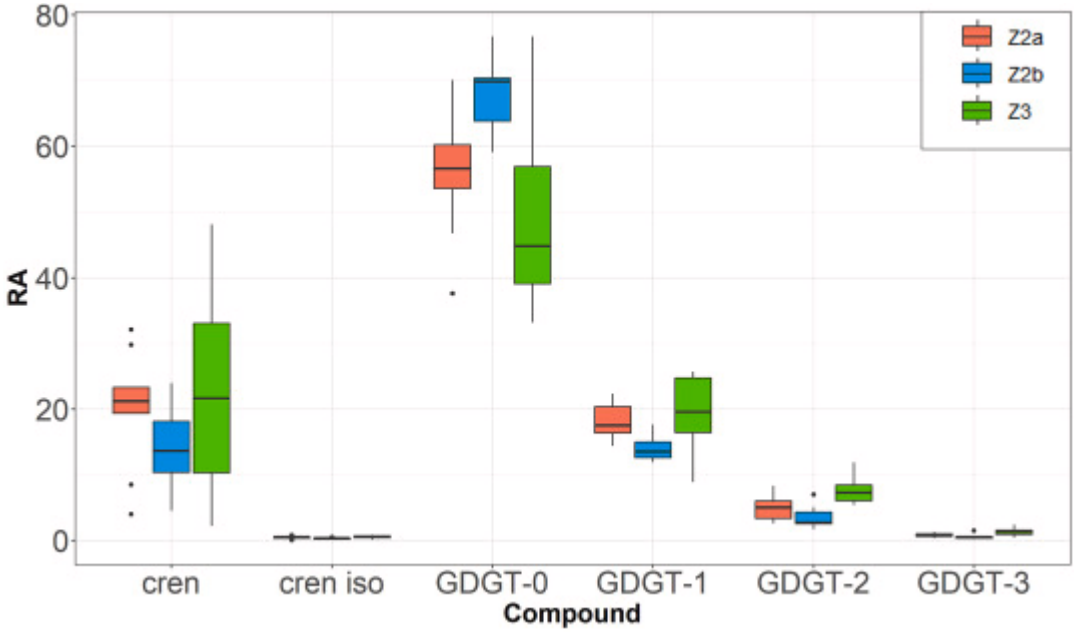

Fig. 5. Relative abundance (RA, %) of isoGDGTs in the lake sediment samples.

Z2a shows the lowest values for GDGT-0/cren ratio (average 2.8 ± 1.7; n = 9).

In Z2b, the relative abundance of GDGT-0 is higher than in the rest of the periods (average 68% ± 5, n = 13), while for the rest of the isoGDGTs compounds Z2b shows the lowest values (Fig. 5), the lowest content of %GDGT-2 (average 18% ± 3.9) and the lowest values in TEX86 (average 0.22 ± 0.04).

In Z3, there is the maximum value of GDGT-0/cren, but also the minimum (30 and 0.7 respectively) throughout the studied record, and there is the lowest relative abundance of GDGT-0 (average 50% ± 13; n = 14). TEX86 values are the highest in Z3 (average 0.31 ± 0.05) and also %GDGT-2 values (average 25.7% ± 4.5) (Table S2).

Periods with high levels of GDGT-0/cren (>7; Fig. 6), were eliminated from the final ALST reconstruction (Fig. 7; see Supplementary Text for details). Those periods ranged between 12.6-12.5; 12.2–12.1; 11.2–10.6; and 9.2 cal ka BP.

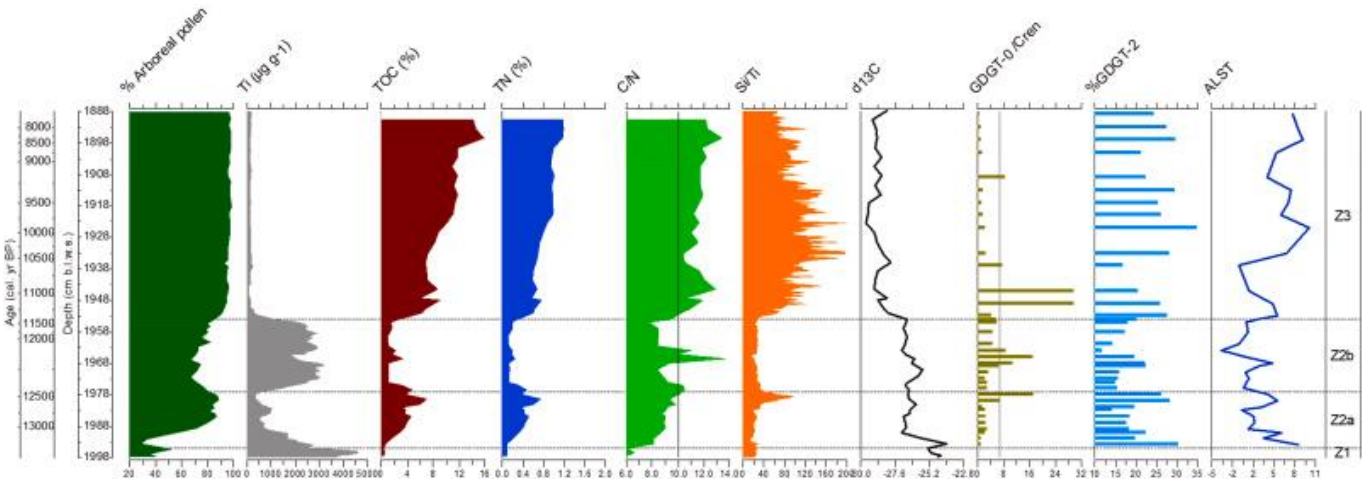

Fig. 6. Multi-proxy diagram for Černé jezero sediment record for the period 13.5–8 cal. ka BP, representing the percentage of arboreal pollen, Ti content, total organic carbon (TOC), total nitrogen content (TN), the carbon-nitrogen ratio (C/N), the silica-titanium ratio (Si:Ti), carbon isotopic composition of bulk sediment (δ13Corg), the GDGT-0 and crenarchaeol ratio (GDGT-0/Chren) where the samples crossing the vertical line correspond to a higher

methanogenic activity, the %GDGT-2 values and ALST based on isoGDGTs which includes the peaks corresponding to the higher methanogenic activity.

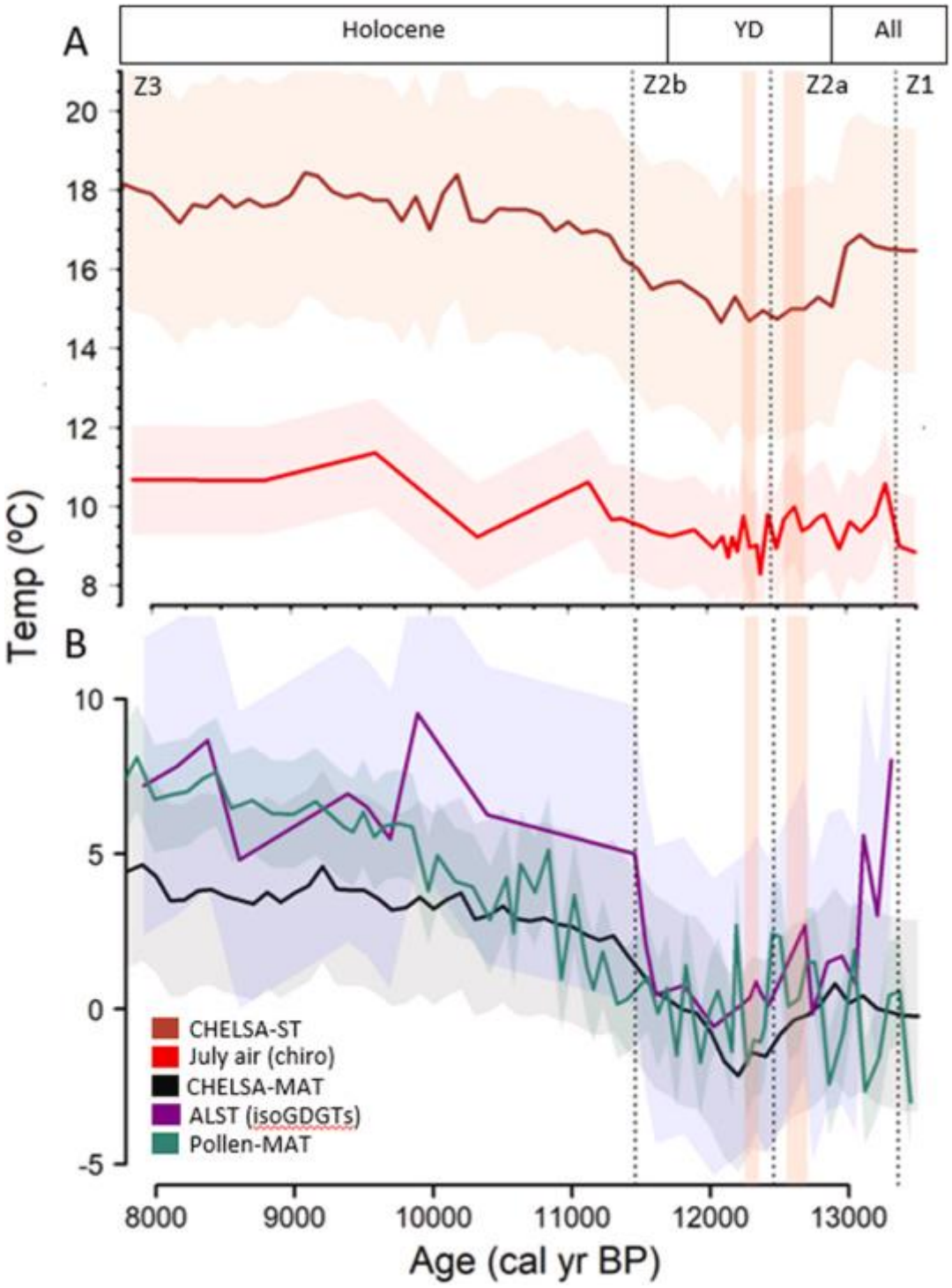

Fig. 7. Modeled and reconstructed temperature series for Černé jezero sediment record from 13.5 to 8 cal. ka BP. A) Mean temperature of the warmest quarter modeled by CHELSA_TraCE21k (Karger et al., 2023) (CHELSA-ST); chironomid-based July mean air temperature (July air (chiro)). B) Mean annual lake surface temperature reconstructed based on the isoprenoid GDGTs proxy eliminating the values during the high peaks in GDGT-0/crenarchaeol (ALST (isoGDGTs)); mean annual temperature modeled by the CHELSA_TraCE21k (CHELSA-MAT); mean annual air temperature modeled by pollen data (Pollen-MAT). The black dotted vertical lines show the zonation of the record based on chironomid data. The red vertical shaded bars represent two identified warmer events during the Younger Dryas. The colored area around each line represents the standard error of the reconstructed values. YD refers to Younger Dryas, and All to Allerød.

In all the samples, the proportion of brGDGTs is higher than isoGDGTs. This is reflected in the high levels of BIT (>0.9; Table S2). In soils, 95% of the GDGTs are branched, while in the lake sediments, there are 82% in Z2a, 85% in Z2b and

89% in Z3. The most abundant brGDGT compound in the lake sediments is GDGT-IIIa, while in the soils is GDGT-Ia (Fig. S4). The brGDGTs IIIa/IIa ratio for the lake sediments samples is between 0.8 and 1.2 and < 0.4 for the soil samples (Fig. S5). The CBT index in soils ranges from 1.2 to 1.7, while in the sediments range from 0.6 to 1.1. The MBT values range from 0.4 to 0.6 in soils and 0.2 to 0.3 in lake sediments. A significant negative correlation between MBT and CBT ($R = -0.66$; p-value = 0.00001) is found in the lake sediment samples. We also evaluate changes in the CBT index values (Fig. S6), which showed large variations from 12.5 to 10.6 cal ka BP, during the Z2b and the beginning of Z3. Therefore, MBT-CBT inferred mean annual air temperatures are not used due to a possible interference of pH changes with the temperature signal (Tyler et al., 2010; De Jonge et al., 2021; Halffman et al., 2022).

3.6. Geochemistry and isotopes

Titanium content (Ti; 65–4619 µg g-1) and biogenic silica (denoted by the Si/Ti ratio; 16 to 197) ranged wider than total organic carbon (TOC; 0.6–15.8%), total nitrogen (TN; 0.08–1.2%), C/N ratio (6–13) and δ13Corg (−29.6 to −24 ‰). Ti shows its highest values in Z1 (13.5–13.35 cal ka BP), contrasting with the low values of TOC, TN, Si/Ti, and C/N (Fig. 6). In Z2a (13.35–12.5 cal ka BP), Ti concentrations rapidly decrease, while TOC, TN, and C/N gradually increase. δ13C values are −27‰ while C/N is ∼8 in this zone. Around 12.85 cal ka BP, there is a brief increase in Ti accompanied by a slight decrease in TOC. Towards 12.5 cal ka BP, TOC, TN, C/N, and Si/Ti suddenly increase while Ti decreased.

Zone 2b (12.5–11.5 cal ka BP) is characterized by a rise and elevated content of Ti. Similar to the other zones, the trends in biological proxies contrast with those in Ti-inferred lithogenic material input, as TOC levels decrease up to 2%, TN decrease up to 0.5%, C/N levels decrease under 10, and Si/Ti levels remain low throughout the zone. However, this trend is interrupted between 1968 and 1963 cm b.l.w.s (ca. 12.15 cal ka BP) with a short-lived decrease in lithogenic input, slightly higher TOC and TN values and an abrupt rise in the C/N ratio, all indicating an input of allochthonous organic material inside the lake.

Zone 3 (11.5–8 cal. ka BP) begins with the highest amplitude changes in the entire geochemical record. There is a sharp decrease in the Ti concentrations, indicating less input of lithogenic material in the lake sediments. The TOC, TN, C/N and Si/Ti ratios gradually increase and remain stable throughout the rest of the zone. The δ13Corg become continually more negative (down to −29‰), indicating a higher rate of biological activity and use of organic carbon in the lake.

3.7. Comparison of proxy-based temperature reconstructions with local modeled temperature

The chironomid-based reconstruction for mean July air temperature ranged from 8.3 to 11.4 °C (Fig. 7). This reconstruction shows the lowest magnitude of change and the narrowest error margin. In comparison with the modeled summer temperatures by CHELSA (CHELSA-ST), which ranged from 14.7 to 18.4 °C, the chironomids present lower absolute values with an average difference of ∼ 7 °C. Moreover, the errors of the reconstructed and modeled summer temperatures do not overlap at any point of the studied period (Fig. 7). CHELSA-ST values for the EH and LG are 6 °C higher than present day summer temperatures, while the values inferred by chironomids for the EH are about 1.5 °C lower than modern ones (12.9 °C).

At 13.5 cal ka BP, July air temperatures inferred by chironomids showed low values (8.9 °C) and increased to 10.5 °C by 13.35 cal ka BP. However, the CHELSA-ST started with temperatures of 16.5 °C and remained stable until a drop by 1.8 °C from 12.9 until 12.1 cal ka BP. For chironomid-based temperatures, there is also a drop by 1.5 °C from 13.3 to 12.95 cal ka BP, while from 12.95 cal ka BP temperatures fluctuated between 9 and 9.8 °C, with a minimum (8.3 °C) around 12.4 cal ka BP. At 12.2 cal ka BP, chironomid inferred temperatures showed another short-term warming by 1.5 °C. It is not until 12.1 cal ka BP, that a continuous and gradual increase in temperatures is obvious in both reconstructed and modeled summer temperature. From 11.5 cal ka BP, reconstructed July temperatures ranged between 9.2 and 11.4 °C, and CHELSA-ST between 16 and 18.4 °C.

The reconstructed and modeled mean annual temperatures presented a higher amplitude of change. ALST (isoGDGTs) reconstruction fluctuated from -0.5 to 9.5 °C. CHELSA-MAT had the lowest amplitude of change from all the annual temperature series, ranging from -2.2 to 4.7 °C. CHELSA-MAT modeled values are lower than ALST throughout the record, especially during the Allerød and EH periods. The pollen-based mean annual temperature reconstruction (pollen-MAT) shows the highest amplitude of change, ranging from -3 to 7.7 °C.

Between 13.5 and 13.3 cal ka BP, pollen-MAT increased from -3 °C to 0.5 °C. At 13.3 cal ka BP, ALST (isoGDGTs) indicates 8 °C. Afterwards, ALST (isoGDGT) shows a decreasing tendency until 13 cal. ka BP when a series of short-term temperature oscillations appeared. Pollen-MAT increased continuously but with high fluctuations until 12.5 cal ka BP, then decreased. For CHELSA-MAT, temperatures oscillated between -0.2 and 0.9 °C until 12.9 cal ka BP, when they decreased gradually. During the YD, the reconstructed and simulated annual temperature series decreased. ALST (isoGDGTs) and CHELSA-MAT reached their minimum values (-0.5 and -2.15 °C respectively) and pollen based MAT reached -1.4 °C around 12.1 cal ka BP. From 12.1 cal ka BP, all annual temperature series rose until the onset of the Holocene, where they stabilized and reached their maximum. However, ALST (isoGDGTs) showed a more rapid increase compared to pollen-MAT and CHELSA-MAT.

3.8. Statistical comparison between reconstructed and modeled temperature series

All the correlations between reconstructed and modeled temperatures presented values >0.5 (Table S1), indicating that the similarity between datasets is higher than expected for random data. CHELSA-MAT and CHELSA-ST presented the highest correlation (R = 0.89). CHELSA-MAT and pollen-MAT also presented a high correlation coefficient (R = 0.68). Chironomids-based July air temperature reconstruction showed the strongest correlation coefficient with CHELSA-ST (R = 0.66). ALST (isoGDGTs) presented the lowest correlation coefficient with chironomid-based temperatures (R = 0.53) and the highest with CHELSA-ST (R = 0.78).

The first two axes of a PCA based on the different temperature series explained 85.2% of the total variability (Fig. 8). The first axis, which explained 74.1% of the total variability, is negatively related to all the modeled and reconstructed temperature series. The second axis, which represented 10.1% of the variation, is negatively correlated with the chironomids July temperature reconstruction and the pollen-based MAT, while the others correlate positively.

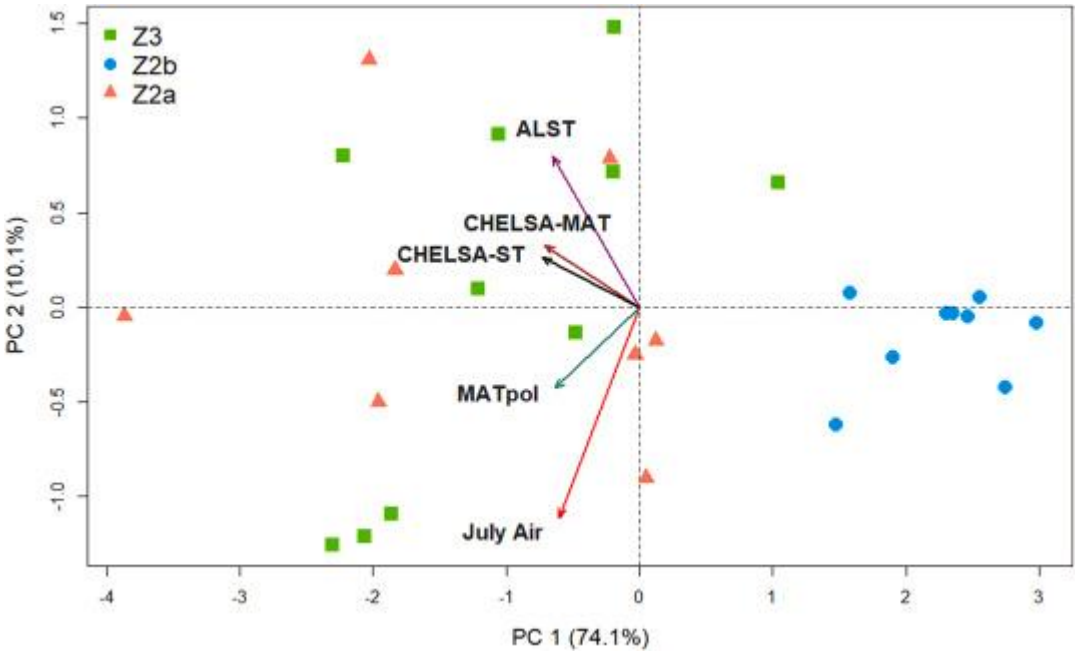

Fig. 8. PCA of the temperature series data. The arrows represent the detrended temperature series, the points represent the samples, and their colour distribution is grouped by zones.

4. Discussion

4.1. Variations in reconstructed and modeled temperature series

We presented three independent temperature proxies and compared them with locally modeled temperature data generated by the CHELSA_Trace21k dataset. Despite the broad range of temperature values shown by the different reconstructions and models (Fig. 7), they all follow a similar trajectory (Fig. 8) and present high correlations between them (Table S1). This suggests they all reflect temperature changes and follow the abrupt climatic changes that occurred during the transition from the LG to the Holocene period. However, each proxy has its limitations which can influence the accuracy of the reconstructed temperature values, and some reconstructions represent different seasons than others (e.g. summer temperature vs. annual temperature reconstructions). For example, differences between chironomids and isoGDGTs temperature reconstructions could be lead by stronger seasonality in the

studied period. It has been proposed that during the LG, the contrast between seasonal temperatures was greater than at present, mainly because of changes in the perihelion and the higher tilt of Earth's axis (Delcourt and Delcourt, 1994). In addition, the YD has been considered a period with strongly continental climate conditions (i.e. a stronger difference between summer and winter temperatures than before or after this period; e.g. Renssen and Isarin, 2001), which could explain some of the disparities between reconstructed July and ALST, and explain to some extent the low amount of inferred change during the YD period by the chironomid based temperatures. Nevertheless, differences in the range of reconstructed temperatures also occurred in proxies which reconstruct the same seasons, as isoGDGTs and pollen-based mean annual temperature reconstructions, which show similar trajectories and high correlations throughout the record (Fig. 8; Table S1), but also discrepancies in the range of reconstructed values (Fig. 7). Below we discuss potential biases within each temperature series to develop a paleoenvironmental reconstruction for the Bohemian Forest during a period of high-amplitude abrupt climatic changes.

4.1.1. Warm bias and methanogenic activity impact the isoGDGT mean annual temperature reconstruction

It has been suggested that isoGDGTs temperature signal often reflects winter temperatures in lakes with high seasonality (Wuchter et al., 2005; Powers et al., 2010) or spring and/or fall temperatures, as this is the time for the overturning in dimictic lakes (Sinninghe Damsté et al., 2022). However, the values of isoGDGT-ALST are higher than the pollen-MAT, especially during the LG. This is noteworthy, as isoGDGTs often show lower values than expected for the mean annual temperatures (Bechtel et al., 2010; Powers et al., 2010; Sinninghe Damsté et al., 2022). This is related to the activity of Thaumarchaeota, whose distribution is more abundant below the thermocline than on the lake surface (Herber et al., 2020; Schouten et al., 2013). Even if the TEX86 index is correlated with lake surface temperatures, in some cases, the distribution of Thaumarchaeota in the deeper parts of the water column can cause a bias in the reconstructed values as the temperature from the bottom is disconnected from the lake surface, leading to lower temperatures (Huguet et al., 2007; Sinninghe-Damsté et al., 2022). However, in Černé jezero isoGDGTs appear biased towards warmer temperatures. It has been observed that low nutrient/productivity sites may lead to warmer reconstructed temperatures based on TEX86, while high nutrient/productivity rates may result in colder biases (Cao et al., 2020). In our record, the levels of nitrogen are low throughout the entire period (TN<2%, Fig. 6) confirming a low-nutrient aquatic environment that likely influenced the activity of Thaumarchaeota, leading to the warmer registered values. Despite the overall high reconstructed temperatures for the LG, isoGDGTs show the most abrupt cooling related to the onset of the YD of all the reconstructed temperature series (Fig. 7), indicating their ability to record such changes. During the YD, the relative abundance of GDGT-0 is the highest (Fig. 5), indicating methanogenic activity at the lake sediments. This may be related to a more persistent ice cover, which would prolong the water stratification period, allowing the methanogenic activity to increase in the sediments (Bertilsson et al., 2013). However, low levels of organic carbon (Fig. 6), entering the lake during this period suggest that microbial activity was not high enough to produce anoxia in the water column (Bertilsson et al., 2013). The low levels of the other isoGDGT compounds could be a consequence of the cold temperatures registered during this period. Thus, even if methanogenic archaea were active in the lake sediments during the YD, its influence on the TEX86 index ability to record the relative changes in temperatures was not strong enough because of the low carbon content. This is appreciable because, even if the relative abundance of GDGT-0 is the highest during the YD, the relative abundances of the rest of the isoGDGT compounds are the lowest (Fig. 5), suggesting that the GDGT-0/cren high levels during the YD were not affecting the TEX86 index. However, in periods when high GDGT-0/cren happened synchronously with an increase in organic carbon, the archaeal activity could interfere with the TEX86 index (See Supplementary Text; Fig. S7). Our findings indicate that it is important to comprehend the distribution of archaea that produce isoGDGTs within the lake system, particularly in oligotrophic cold lakes where the low organic content may restrict anoxic activity, enabling the TEX86 index to reflect the relative temperature variations.

4.1.2. The effect of water depth on chironomid-based July air temperature reconstruction

The July air temperature reconstruction based on subfossil chironomids indicates less pronounced changes than the mean annual temperature reconstructions. This is expected as the signals of chironomids, isoGDGTs and pollen reflect different seasons. Even though chironomids seem to capture the variability in July air temperatures (Fig. 7), temperature values are relatively low and there likely exists a possible cold bias from this reconstruction. For example, at 9.6 cal ka BP, chironomid-based July air temperatures reached their maximum of 11.4 °C (Fig. 7), which is still lower than the modern values (12.9 °C; Turek et al., 2014). However, the vegetation at that time was composed of more thermophilous taxa than nowadays, such as Corylus avellana and Quercus (Fig. 4). The predominance of

cold-preference chironomid species in the EH can possibly also be attributed to the lake's depth, as many of these taxa can inhabit cold and deep water layers in deep lakes, even under relatively warm summer climates, while the warmer-indicating taxa colonized the littoral zone in the same habitats (Brooks et al., 2007). With a water depth of 40.1m, Černé jezero is a significantly deeper lake than some of the lakes that form the calibration dataset used for the chironomid-based temperature inference model, even though it is still in the range of depths inside the Swiss calibration dataset (2.1–85 m; Heiri et al., 2011). This may have led to reconstructed temperatures that are cooler than the actual temperatures that existed at the lake in the past. Lakes characterized by cooler summer water temperatures than expected based on the ambient summer air temperatures may be colonized by cold adapted chironomid species and characterized by too low reconstructed temperature values (e.g. Brooks and Birks, 2001). Therefore, even if the climatic trend presented by the chironomids-based temperature reconstruction is accurate, the values of the reconstruction show colder temperatures than what is expected in this kind of lake.

4.1.3. Regional and growing season signals as potential impacts on pollen mean annual temperature reconstruction

Our pollen temperature reconstruction seems to register a lagged effect on increasing temperatures at the onset of the Holocene. In contrast, chironomid and isoGDGTs temperature reconstructions react quickly to the increase of the temperatures (Fig. 7). This slower response could be caused by the longer period for vegetation to respond to climate change (e.g. trees grow, biomes change, trees to become large pollen producers), meanwhile for chironomid head capsules or lipid biomarkers it takes shorter time (Wischnewski et al., 2011). In addition, pollen-based quantitative temperature reconstructions in mountainous regions may be affected by phenomena such as the uphill transport of tree pollen by wind (Ortu et al., 2006) compared to low and middle elevations. Pollen temperature reconstructions are based on regional scales (Wischnewski et al., 2011; Ding et al., 2019); meanwhile, chironomids and isoGDGTs originate inside the lake, reflecting a more local signal. Finally, in the northern hemisphere, where we gathered all of our modern pollen data (Fig. S1), the temperature during the summer season is the limiting factor for growth and therefore drives vegetation changes (Rehfeld et al., 2016). Thus, pollen-based temperature reconstruction, even if calibrated versus annual temperatures, may be biased to some extent towards the growing season. This is reflected in our data by the fact that the pollen-based temperature reconstruction did not capture the abrupt decrease of temperatures associated with the onset of the YD, as isoGDGTs, but as a small decrease, as chironomids captured it.

4.1.4. Comparing local proxy-based records with CHELSA model

Despite the strong correlation and similar long-term trend between the CHELSA-modeled and proxy-based temperature series some differences are apparent (Fig. 7). For example, the CHELSA-MAT, pollen-MAT, and ALST isoGDGTs-based temperature reconstruction show pronounced cooling during the YD and abrupt warming at the Holocene onset (Fig. 7). Conversely, CHELSA-ST and chironomid-inferred July temperature show the largest difference in absolute values, with the CHELSA-ST exceeding the present-day temperatures by ~ 6 °C. Thus, it is most likely that modeled local summer temperatures for the LG and EH are overestimated, as such high temperatures also do not agree with the boreal vegetation recorded at the site during the LG (Fig. 4). This difference can be attributed to stronger summer insolation during the LG than today (Berger and Loutre, 1997), which cause an exaggeration of the summer modeled temperatures with higher-than-present summer values (12.9 °C, Turek et al., 2014). Despite its 1 km-grid resolution, the CHELSA-ST modeled temperatures do not appear to capture local climate deviations reconstructed by local proxy-based models. Additionally, the difference between CHELSA-ST and proxy-based temperatures may also be associated with the complex topography within the Bohemian Forest which may be over-simplified in the CHELSA-based model. Elevation of Černé jezero and the irregular morphometry of its basin and catchment favour thermal inversions (Svobodová et al., 2001) that would not be captured by the CHELSA model.

4.2. Late Glacial to Early Holocene climatic variation and related environmental changes

We have cross-checked our results with sequences from other Central European records and the Greenland ice-core record (NGRIP) to validate our age-depth model (Fig. 9). The synchronicity of some temperature oscillations between our record and others supports the precision of our age-depth model. However, it's worth noting that some of the dated samples in the oldest section of our sedimentary record may have been impacted by periods of constant 14C age, or "radiocarbon plateaus" (Lowe et al., 2008).

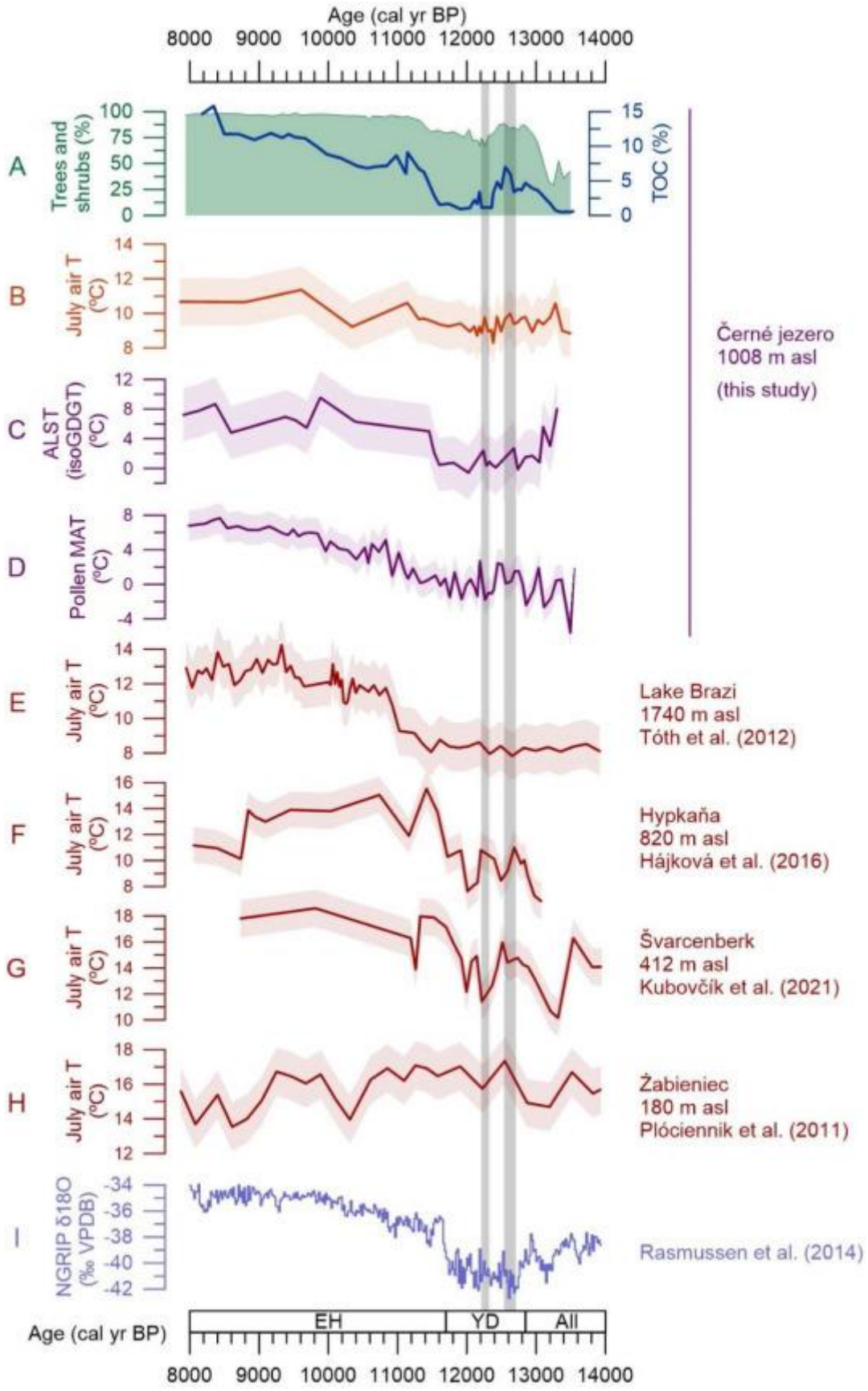

Fig. 9. Synthesis of temperature records from our study (B, C and D) and comparison with other areas during the LG and EH. Graph A shows the percentage of arboreal pollen and the percentage of TOC in the lake sediments of Černé jezero. Vertical bars indicate the short warm oscillations during the YD. Temperature reconstructions from E to H are based on chironomids and reconstruct July air temperatures in the referenced areas.

4.2.1. Allerød (13.9–12.85 cal ka BP)

Between 13.5 and 13.35 cal ka BP, the chironomid record from Černé jezero indicates cold and ultra oligotrophic conditions typical of subarctic areas (Brooks et al., 2007) with summer temperatures around 9 °C (Fig. 7). Low levels of TOC and TN (<1% and <0.5%), suggest non-developed catchment soils and low productivity or biological activity in the lake (Fig. 6). High levels of Ti imply high rates of physical erosion which are associated with bare soils (Hošek et al., 2017), suggesting an open, treeless environment. Pollen-based vegetation was characteristic of cold steppes and tundra comprising mainly herbaceous plants and some shrubs such as Juniperus and Betula nana (Kuneš et al., 2008). Nevertheless, the occurrence of Picea abies pollen throughout the record (Fig. 4), although in low numbers, indicates that the species could have been present in the immediate area instead of their pollen being transported over long distances (Jankovská, 2006; Tollefsrud et al., 2008; Vočadlová et al., 2015).

Around 13.35 cal ka BP, a significant climate amelioration is visible in the reconstructed palaeotemperature records, with ALST indicating a mean annual temperature of ~8 °C, while chironomid inferred-July temperature increases by 1.5 °C (Fig. 7). This amelioration of the climatic conditions is seen in the expansion of the vegetation cover, primarily driven by the rapid response of the herbaceous plants to the improved conditions (Fig. 4). The slightly elevated macro-charcoal influx further supports occasional burning of local vegetation (Fig. 4). This resulted in a gradual decrease in lithogenic input to the lake as the soils became more stabilized by the expanding vegetation cover (Fig. 6).

4.2.2. Younger Dryas (12.85–11.7 cal ka BP)

The Younger Dryas has been identified as a biostratigraphic unit, characterized by a decrease in arboreal PAR due to abrupt decreases in temperatures (Engels et al., 2022). In Western Europe it had a distinct and noticeable onset, as the decrease in temperatures and in arboreal PAR was synchronous (Heiri et al., 2014; Engels et al., 2022). However, it was not as marked in Eastern European regions with a continental climate (Płóciennik et al., 2011; Tóth et al., 2012). In the Bohemian Forest, this decrease in temperatures is difficult to assess due to uncertainties in the age-depth model. However, an abrupt decrease in mean annual temperatures occurred around 13 cal. ka BP, when isoGDGTs inferred-ALST decreased by almost 5 °C, while July air temperatures inferred from chironomids decreased only by 0.7 °C (Fig. 7). Thus, mild temperatures during the growing season at this time likely contributed to the increase in arboreal pollen from 30% to 85% (Fig. 6). Vegetation of open habitats, such as Helianthemum and Brassicaceae, disappeared, while Pinus increased (Fig. 4), suggesting a mixture of shrub and steppe patches with scattered pine trees (Kuneš et al., 2008; Pokorný, 2002). This indicates that proxies which record the summer temperatures (chironomids) or growing season (pollen) do not respond as strongly to the climatic changes during the YD as proxies recording annual temperatures. As the decrease in temperatures was apparently less pronounced during the summer season (Fig. 7), vegetation did not show a synchronous response to the main cooling trend (Fig. 4). This discrete response to the YD cooling is also found in other Eastern European records (Żabieniec in Poland and Lake Brazi in Romania; Fig. 1A; Fig. 9). At Lake Brazi, chironomid-inferred July temperatures decreased by < 1 °C (Tóth et al., 2012) but the ice-cover season was longer (Buczkó et al., 2012), indicating that the temperature decrease during the YD could have been stronger during the winter season and less noticeable during the summer. Furthermore, Heiri et al. (2014) showed that chironomid inferred summer cooling during the YD was very small in Eastern Europe compared with more westerly parts of the continent. Our results agree with these earlier results, with mean annual temperatures showing a larger decrease than July temperatures alone, suggesting a considerably more pronounced cooling during the winter and possibly also spring and autumn months than during summer. Around 12.85 cal ka BP, there is a slight decrease in isoGDGTs-based ALST of 1 °C and in chironomid-inferred July temperature of 0.5 °C. At this time the biota and environments responded to the cooling modestly, with a small increase in herbaceous plants, mainly Poaceae and Artemisia (Fig. 4), and a slight decrease in TOC and lithogenic input (Fig. 6). However, at 12.4 cal ka BP, chironomid-inferred July air temperatures decreased by ca. 2 °C to their minimum, while pollen assemblages strongly responded to the YD cooling by a major decrease in arboreal pollen and the reappearance of cold adapted species such as Dryas octopetala.

Possibly minor warm oscillations may have interrupted the overall cooling during the YD in Central-Eastern Europe. This may have promoted short-term expansions of arboreal species at Černé jezero and the non-synchronous response of the pollen assemblages to the cooling temperatures which characterize the onset of the YD. Previous studies have suggested some rapid warming episodes during the YD in Central Europe. Schwark et al. (2002; Fig. 1A) proposed a ‘Middle Younger Dryas Warming’ around 12.3–12.2 cal ka BP, when they detected an increase in

terrestrial higher plants n-alkanes (>n-C25), such as n-C27 alkane indicative of major presence of Betula. Chironomid-based temperature reconstructions from Eastern Slovakia (Hájková et al., 2016, Figs. 1A and 9) suggested two warmer episodes between 12.85 and 12.6 cal ka BP and 12.4–12.2 cal ka BP. Furthermore, in South Bohemia (Kubovčík et al., 2021) (Fig. 1A; Fig. 9), chironomid-reconstructed July temperatures showed relatively minor temperature increases at 12.5 cal ka BP and 12.2 cal ka BP. In both cases, these warmer episodes coincided with lower water levels, which prompts further investigation of these two warm episodes. At Černé jezero, both chironomid and isoGDGT-based temperature reconstructions record a first warming event around 12.6 cal ka BP, with a relatively minor July air temperature increase by 0.6 °C and a more pronounced mean annual temperature increase of 2.3 °C (Fig. 7). During this event, there is a significant increase in phytoplanktonic activity within the lake system suggested by the increase in the Si/Ti ratio (Fig. 6). In the absence of biological activity, the Si/Ti ratio is constant and derives from the erosion of bedrock. However, diatoms use and incorporate silica as an essential component of their frustules, thereby increasing the ratio values (Peinerud, 2000). An increase in phytoplankton is also supported by the presence of other algae colonies, mainly Botryococcus (Fig. 4). At ca. 12.6 cal ka BP increases in the C/N ratio indicate an increase in the amount of organic material coming from the catchment (Fig. 6). GDGT-0/cren also increased at ca. 12.6 cal ka BP (Fig. 6), likely in response to increasing organic material input and subsequently higher activity of the archaeal community. As the lake has an extensive area and low trophic level, an increase in the anaerobic environment does not necessarily imply eutrophication, but instead an expansion of the anoxic sediments. There was no significant difference in the chironomid assemblages, which could support anoxic conditions in the entire lake (Fig. 3), suggesting that oxygen depletion and methanogenic activity would have been restricted to sediments of the deepest parts of the lake.

The second warm event was recorded around 12.2 cal ka BP with a July temperature increase of 1.5 °C, and ALST (isoGDGT) increase of 4 °C (Fig. 7). During both warming events, the isoGDGTs temperature reconstruction was affected by high levels of GDGT-0/cren, making it difficult to explore quantitatively the increase of temperatures (Fig. 6). It has been suggested that the YD stadial in Central Europe may have consisted of two phases: an older one marked by colder and drier conditions and a subsequent phase with warmer, wetter climate (Kubovčík et al., 2021; Pokorný, 2002). This is supported by our palaeotemperature record, showing temperature fluctuations and minimum values during the older phase, followed by a gradual temperature rise across all reconstructions. These short-lived warm events during the first part of the YD, along with drier conditions and overall very little decrease in the summer temperatures, could explain why there was no regrowth of the continental ice-glacier in the Bohemian Forest during the YD period (Mentlík et al., 2013). During the transition between these two YD phases, when the environment changed from drier to wetter (Pokorný, 2002), a second peak in methanogenic archaeal activity occurred. During the YD, the biological activity in the catchment and within the lake was low, as is shown by low levels of TOC and TN, except for a peak in TOC, TN and C/N around 12.1 cal ka BP (Fig. 6). Thus, some organic material entered the lake but there was no response from primary producers (neither Si/Ti nor algae in the pollen record), as only the methanogenic archaea reacted along with a depletion of $\delta^{13}C_{org}$. During this period, there was also a decrease in lithogenic input to the lake, which excludes a possible landslide as the cause of this increment in organic material. This decrease in lithogenic input ~12.1 cal ka BP has been also recorded in southern parts of the Czech Republic (Hošek et al., 2017; Kubovčík et al., 2021) and has been attributed to an increase in precipitation. In the case of Černé jezero, there is a simultaneous increase in fern spores and very low charcoal influx (Fig. 4) at that time, which could be related to increasing moisture creating suitable habitats for ferns and less fire-prone conditions. During the YD, the lake had low levels of organic carbon. Therefore, even small changes in the catchment area, like an increase in ferns leading to higher influx of organic carbon to the lake, could have had a significant effect on the lacustrine communities. This might have increased methanogenic activity as the archaea may have made rapid use of the organic carbon, depleting the sediments oxygen level (Harvey et al., 1986).

4.2.3. Early Holocene (11.7–8.0 cal ka BP)

The onset of the Holocene in Černé jezero occurred around 11.5 cal ka BP and it was characterized by a remarkable change in the ecosystem, similar to other locations in which biological activity was also limited by low temperatures (Clark et al., 2012; Feurdean et al., 2014). July temperature as inferred by chironomids rose by 1 °C in 400 years, and the ALST isoGDGTs-based temperature increased by 2 °C in the same period (Fig. 7). The improved climatic conditions and the possible extension of the growing season resulted in a blooming of biological activity in the terrestrial and aquatic environment at the beginning of the EH. The area became more forested as light-demanding herbs disappeared, such as Helianthemum nummularium-type. Tree taxa, dominated by Betula and Pinus sylvestris-type,

expanded at the expense of shrub communities (Fig. 4). Tree/shrub growth inside the lake catchment is supported by a notable increase in macroscopic charcoal influx from 11.2 cal ka BP, suggesting an abundant fuel load and increased fire activity (Fig. 4). By 11.0–10.5 cal ka BP, a mixed-deciduous forest developed, with mesophilic species such as Corylus avellana, Picea abies, and Quercus (Fig. 4). With soil and vegetation cover development, the input of lithogenic material stabilized to a minimum (Fig. 6). The lake biota reacted fast to temperature changes due to the previous scarcity of organic resources. Černé jezero was a relatively large and ultraoligotrophic water body, so the increase in organic resources, even if small, was rapidly assimilated by the living biota.

Warmer temperatures at 11.5 cal ka BP resulted in a rapid increase in chironomid diversity (Fig. 3). The phytoplanktonic activity increased, as indicated by the Si/Ti ratio, and methanogenic activity reached its highest peak between 11.3 and 10.6 cal ka BP, as shown by the GDGT-0/cren ratio (Fig. 6). The bottom water and sediments could have been affected by oxygen depletion between 11.3 and 10.4 cal ka BP, as evidenced by a decrease of the chironomids' head capsules and by a shift to more depleted δ13Corg during the peak of GDGT-0/cren (Teranes and Bernasconi, 2005) (Fig. 6). Strongly depleted bulk sediment values of δ13Corg can indicate an increase in phytoplanktonic respiration rate and also a significant contribution of methanotrophic bacteria biomass, as the methanotrophs fractionate between −16‰ and −30‰ during biosynthesis when utilizing methane which is already strongly depleted in δ13Corg (Summons et al., 1994; Whiticar, 1999). Thus, the decrease in δ13Corg from −26‰ to −29‰ at the onset of the Holocene may be related to the increase in microbial activity, influenced by an increase in both phytoplanktonic and methanogenic activity. Warmer temperatures along with enhanced delivery of organic matter from the lake catchment area may have jointly contributed to the installation of anoxic conditions. Nevertheless, around 10.6 cal ka BP, there was an enrichment of δ13Corg, indicating improving oxygen availability and less anaerobic activity.

The temperature reconstructions inferred by biological proxies reached their maxima during EH, with ALST inferred by isoGDGTs at 9.9 cal ka BP and chironomid-based July temperatures at 9.6 cal ka BP. Maximum temperatures inferred by pollen appeared later, around 8.5 cal ka BP. The amelioration of the climatic conditions allowed mesophilic tree species, such as Corylus or Quercus, to expand and dominate the landscape. Canopy density increased, as shown by a gradual decline of upland herbs and an increase in mixed deciduous forest taxa (Fig. 4). Warmer fire-prone conditions, together with the increasing biomass, and especially the establishment of Picea abies (Bobek et al., 2018; Carter et al., 2018b) in the lake catchment may have led to increasing biomass burning that peaked at 9.3 cal ka BP. At the same time, the increase in GDGT-0/cren and lower Si/Ti ratios (Fig. 6) which might indicate a decrease in photosynthetic activity. A high macro-charcoal influx, associated with a correspondingly high decrease in tree (particularly spruce) pollen abundance (Fig. 4) are indicative of high-severity fires which could generate sufficient ash to reduce water transparency and therefore affect the photosynthetic activity in the epilimnion. This would have affected not only the primary producers' activity but also the community composition in the deeper layers of the lake (Scordo et al., 2021), decreasing the Thaumarchaeota activity. After this period of increased fire activity, tree species gradually recovered, with the dominance of Picea abies and Alnus. The increase in pollen influx of the mesophilic species and organic carbon indicates a post-fire recovery and the prevalence of the mixed deciduous forest for the rest of the Early Holocene.

5. Conclusions

Our study used three independent proxy records to reconstruct the Late Glacial and Early Holocene temperatures for a mountain lake system in Central Europe. Chironomid, isoGDGT and pollen-inferred temperatures exhibit similar patterns and confirm the reliability of the reconstructions, particularly the pattern of change, despite reflecting different seasonal signals and, therefore, different amplitudes of temperature variation. Chironomids, isoGDGTs and pollen-based reconstructions converge in identifying several climatic tendencies, showing a decrease in temperatures from 13.3 to 13 cal. ka BP, and an increase in temperatures at the onset of the Holocene around 11.5 cal ka BP. The cooling trend related to the onset of the Younger Dryas was more pronounced in mean annual reconstructed temperatures than during July, confirming high seasonality during this period with cold and long winters and relatively warm and short summers. This cooling was followed by a series of climatic oscillations and short-term warm events, along with a low decrease in temperatures during the growing season caused a non-synchronous environmental response to the YD compared to many other described European records. Even though chironomids, isoGDGTs and pollen had similar trends, some discrepancies were also inherent in the reconstructions, proving that

paleoclimatic studies can be enriched from a multi-proxy approach. We found that ALST inferred by isoGDGTs was likely affected by methanogenic activity during different periods, even though the TEX86 signal was only affected when the methanogenic activity was accompanied by an increase in organic content entering the lake system. The chironomid-based temperature reconstruction also showed some constraints, likely associated with a cold bias as a consequence of the depth of the lake. Finally, the pollen temperature reconstruction using the RF technique showed a lag in response to the temperature trends in comparison to chironomids and isoGDGTs, indicating a more regional signal. As opposed to the proxy-based temperature series, the CHELSA-ST reconstructed temperatures for the LG were higher than present-day values while CHELSA-MAT variability generally matched the annual values reconstructed from isoGDGTs. The temperature records provided by this study support the idea that in areas far from the North Atlantic climatic influence, the cooling effect of the Younger Dryas was less significant during the summer season (Renssen and Isarin, 2001; Feurdean et al., 2014; Heiri et al., 2014). Furthermore, the beginning of this stadial in the Bohemian Forest and other areas in Central Europe was interrupted by several short-term oscillations which delayed the response of the communities to the large-scale cooling pattern.

Declaration of competing interest

The authors declare that they have no known competing financial interests or personal relationships that could have appeared to influence the work reported in this paper.

Acknowledgement

This research was supported by the Czech Science Foundation, projects BESTFORCE no. 20-13368S and BOBAFIRES no. 19-14271Y. We thank the Šumava National Park administration and the landowners of the Czech State Forest for allowing us to perform the research activities at the lake, and to John Boyle, Jennifer Clear, Fiona Russell, Daniel Schillereff, and Daniel Vondrák for assistance during the coring. We thank Anežka Skurčáková for the identification of the chironomid head capsules for the LG period. We thank Ulrich Treffert for support in the organic geochemistry laboratory in Frankfurt. We are also grateful to Jaroslav Kukla and Kateřina Jandová for their help with the isotopic analysis. Some of the equipment used for this study was purchased from the Operational Programme Prague - Competitiveness (Project CZ.2.16/3.1.00/21516). This work was also supported by the Laboratory Directed Research and Development program at Los Alamos National Laboratory under project number 20230864PRD3. Lastly, we would like to thank the reviewers, Marta Rodrigo-Gámiz and an anonymous reviewer, and the Editor, Donatella Magri, for their helpful and constructive comments and suggestions.

References

Alley R.B. 2000. The Younger Dryas cold interval as viewed from central Greenland, Quaternary Science Reviews, 19, 45413, 213-226

Bechtel A., Smittenberg R.H., Bernasconi S.M., Schubert C.J. 2010. Distribution of branched and isoprenoid tetraether lipids in an oligotrophic and a eutrophic Swiss lake: Insights into sources and GDGT-based proxies, Organic Geochemistry, 41, 8, 822-832

Bennett K.D. 1996. Determination of the number of zones in a biostratigraphical sequence, New Phytologist, 132, 1, 155-170

Bennett K.D. 1993. PSIMPOLL 2.27: Program for plotting pollen diagrams and analysing data

Berger A., Loutre M.F. 1997. Long-term variations in insolation and their effects on climate, the LLN experiments, Surveys in Geophysics, 18, 45353, 147-161

Bertilsson S., Burgin A., Carey C.C., Fey S.B., Grossart H.-P., Grubisic L.M., Jones I.D., Kirillin G., Lennon J.T., Shade A., Smyth R.L. 2013. The under-ice microbiome of seasonally frozen lakes, Limnology and Oceanography, 58, 6, 1998-2012

Beug H.J. 2004. [No title available], Leitfaden der Pollenbestimmung für Mitteleuropa und angrenzende Gebiete, 542

Birks H.H., Birks H.J.B. 2014. To what extent did changes in July temperature influence Lateglacial vegetation patterns in NW Europe?, Quaternary Science Reviews, 106 262-277

Birks H.H., Birks H.J.B. 2006. Multi-proxy studies in palaeolimnology, Vegetation History and Archaeobotany, 15, 4, 235-251

Birks H.H., Ammann B. 2000. Two terrestrial records of rapid climatic change during the glacial- Holocene transition (14,0009,000 calendar years B.P.) from Europe, Proceedings of the National Academy of Sciences of the United States of America, 97, 4, 1390-1394

Blaauw M., Christeny J.A. 2011. Flexible paleoclimate age-depth models using an autoregressive gamma process, Bayesian Analysis, 6, 3, 457-474

Blaga C.I., Reichart G.-J., Heiri O., Sinninghe Damsté J.S. 2009. Tetraether membrane lipid distributions in water-column particulate matter and sediments: A study of 47 European lakes along a north-south transect, Journal of Paleolimnology, 41, 3, 523-540

Bobek P., Šamonil P., Jamrichová E. 2018. Biotic controls on Holocene fire frequency in a temperate mountain forest, Czech Republic, Journal of Quaternary Science, 33, 8, 892-904

Boyle J., Chiverrell R., Schillereff D. 2015. Approaches to water content correction and calibration for µXRF core scanning: comparing x-ray scatter with simple regression of elemental concentrations, Developments in Palaeoenvironmental Research: Micro-XRF Studies of Sediment Cores, 17, 373-390

Brooks S.J., Langdon P.G., Heiri O. 2007. The Identification and Use of Palaearctic Chironomidae Larvae in Palaeoecology

Brooks S.J. 2006. Fossil midges (Diptera: Chironomidae) as palaeoclimatic indicators for the Eurasian region, Quaternary Science Reviews, 25, 15-16, 1894-1910

Brooks S.J., Birks H.J.B. 2001. Chironomid-inferred air temperatures from Lateglacial and Holocene sites in north-west Europe: Progress and problems, Quaternary Science Reviews, 20, 16-17, 1723-1741

Brooks S.J. 1997. The response of Chironomidae (Insecta: Diptera) assemblages to late-glacial climatic change in Kråkenes Lake, western Norway, Quaternary Proceedings, 5, 49-58

Brown E.T. 2015. Estimation of biogenic silica concentrations using scanning XRF: insights from studies of Lake Malawi sediments, Micro-XRF Studies of Sediment Cores, 267-277

Buczkó K., Magyari E., Hübener T., Braun M., Bálint M., Tóth M., Lotter A.F. 2012. Responses of diatoms to the Younger Dryas climatic reversal in a South Carpathian mountain lake (Romania), Journal of Paleolimnology, 48, 2, 417-431

Butiseacă G.A., van der Meer M.T.J., Kontakiotis G., Agiadi K., Thivaiou D., Besiou E., Antonarakou A., Mulch A., Vasiliev I. 2022. Multiple crises preceded the Mediterranean Salinity Crisis: Aridification and vegetation changes revealed by biomarkers and stable isotopes, Global and Planetary Change, 217

Cao M., Rivas-Ruiz P., Trapote M.D.C., Vegas-Vilarrúbia T., Rull V., Rosell-Melé A. 2020. Seasonal effects of water temperature and dissolved oxygen on the isoGDGT proxy (TEX86) in a Mediterranean oligotrophic lake, Chemical Geology, 551

Carter V.A., Moravcová A., Chiverrell R.C., Clear J.L., Finsinger W., Dreslerová D., Halsall K., Kuneš P. 2018. Holocene-scale fire dynamics of central European temperate spruce-beech forests, Quaternary Science Reviews, 191, 15-30

Carter V.A., Chiverrell R.C., Clear J.L., Kuosmanen N., Moravcová A., Svoboda M., Svobodová-Svitavská H., Van Leeuwen J.F.N., Van Der Knaap W.O., Kuneš P. 2018. Quantitative palynology informing conservation ecology in the bohemian/bavarian forests of central europe, Frontiers in Plant Science, 8 -

Castañeda I.S., Schouten S. 2011. A review of molecular organic proxies for examining modern and ancient lacustrine environments, Quaternary Science Reviews, 30, 21-22, 2851-2891

Chevalier M., Davis B.A.S., Heiri O., Seppä H., Chase B.M., Gajewski K., Lacourse T., Telford R.J., Finsinger W., Guiot J., Kühl N., Maezumi S.Y., Tipton J.R., Carter V.A., Brussel T., Phelps L.N., Dawson A., Zanon M., Vallé F., Nolan C., Mauri

A., de Vernal A., Izumi K., Holmström L., Marsicek J., Goring S., Sommer P.S., Chaput M., Kupriyanov D. 2020. Pollen-based climate reconstruction techniques for late Quaternary studies, Earth-Science Reviews, 210 -

Čížková P., Svoboda M., Křenová Z. 2011. Natural regeneration of acidophilous spruce mountain forests in non-intervention management areas of the Šumava National Park - The first results of the Biomonitoring project, Silva Gabreta, 17, 1, 19-35

Clark P.U., Shakun J.D., Baker P.A., Bartlein P.J., Brewer S., Brook E., Carlson A.E., Cheng H., Kaufman D.S., Liu Z., Marchitto T.M., Mix A.C., Morrill C., Otto-Bliesner B.L., Pahnke K., Russell J.M., Whitlock C., Adkins J.F., Blois J.L., Clark J., Colman S.M., Curry W.B., Flower B.P., He F., Johnson T.C., Lynch-Stieglitz J., Markgraf V., McManus J., Mitrovica J.X., Moreno P.I., Williams J.W. 2012. Global climate evolution during the last deglaciation, Proceedings of the National Academy of Sciences of the United States of America, 109, 19, E1134-E1142

Clark P.U., Marshall S.J., Clarke G.K.C., Hostetler S.W., Licciardi J.M., Teller J.T. 2001. Freshwater forcing of abrupt climate change during the last glaciation, Science, 293, 5528, 283-287

Čtvrtlíková M., Kopáček J., Nedoma J., Znachor P., Hekera P., Vrba J. 2023. Aquatic quillworts, Isoëtes echinospora and I. lacustris under acidic stress—A review from a temperate refuge, Ecology and Evolution, 13, 3, -

Davis B.A.S., Chevalier M., Sommer P., Carter V.A., Finsinger W., Mauri A., Phelps L.N., Zanon M., Abegglen R., Åkesson C.M., Alba-Sánchez F., Scott Anderson R., Antipina T.G., Atanassova J.R., Beer R., Belyanina N.I., Blyakharchuk T.A., Borisova O.K., Bozilova E., Bukreeva G., Jane Bunting M., Clò E., Colombaroli D., Combourieu-Nebout N., Desprat S., Di Rita F., Djamali M., Edwards K.J., Fall P.L., Feurdean A., Fletcher W., Florenzano A., Furlanetto G., Gaceur E., Galimov A.T., Gałka M., García-Moreiras I., Giesecke T., Grindean R., Guido M.A., Gvozdeva I.G., Herzschuh U., Hjelle K.L., Ivanov S., Jahns S., Jankovska V., Jiménez-Moreno G., Karpińska-Kołaczek M., Kitaba I., Kołaczek P., Lapteva E.G., Latałowa M., Lebreton V., Leroy S., Leydet M., Lopatina D.A., López-Sáez J.A., Lotter A.F., Magri D., Marinova E., Matthias I., Mavridou A., Mercuri A.M., Mesa-Fernández J.M., Mikishin Y.A., Milecka K., Montanari C., Morales-Molino C., Mrotzek A., Sobrino C.M., Naidina O.D., Nakagawa T., Nielsen A.B., Novenko E.Y., Panajiotidis S., Panova N.K., Papadopoulou M., Pardoe H.S., Pędziszewska A., Petrenko T.I., Ramos-Román M.J., Ravazzi C., Rösch M., Ryabogina N., Ruiz S.S., Sakari Salonen J., Sapelko T.V., Schofield J.E., Seppä H., Shumilovskikh L., Stivrins N., Stojakowits P., Svitavska H.S., Święta-Musznicka J., Tantau I., Tinner W., Tobolski K., Tonkov S., Tsakiridou M., Valsecchi V., Zanina O.G., Zimny M. 2020. The Eurasian Modern Pollen Database (EMPD), version 2, Earth System Science Data, 12, 4, 2423-2445

De Jonge C., Kuramae E.E., Radujković D., Weedon J.T., Janssens I.A., Peterse F. 2021. The influence of soil chemistry on branched tetraether lipids in mid- and high latitude soils: Implications for brGDGT- based paleothermometry, Geochimica et Cosmochimica Acta, 310 95-112

Delcourt H.R., Delcourt P.A. 1994. Postglacial rise and decline of Ostrya virginiana (Mill.) K.Koch and Carpinus caroliniana Walt. in eastern North America: Predictable responses of forest species to cyclic changes in seasonality of climates, Journal of Biogeography, 21, 2, 137-150

Ding W., Xu Q., Fu T., Ma C., Tarasov P.E. 2019. Heterogeneous vegetation sensitivity at local and regional scales: Implications for pollen-based climate reconstruction, Quaternary International, 516 149-159

D'Oliveira L., Dugerdil L., Ménot G., Evin A., Muller S.D., Ansanay-Alex S., Azuara J., Bonnet C., Bremond L., Shah M., Peyron O. 2023. Reconstructing 15 000 years of southern France temperatures from coupled pollen and molecular (branched glycerol dialkyl glycerol tetraether) markers (Canroute, Massif Central), Climate of the Past, 19, 11, 2127-2156

Eggermont H., Heiri O. 2012. The chironomid-temperature relationship: Expression in nature and palaeoenvironmental implications, Biological Reviews, 87, 2, 430-456

Engels S., Lane C.S., Haliuc A., Hoek W.Z., Muschitiello F., Baneschi I., Bouwman A., Bronk Ramsey C., Collins J., de Bruijn R., Heiri O., Hubay K., Jones G., Laug A., Merkt J., Müller M., Peters T., Peterse F., Staff R.A., ter Schure A.T.M., Turner F., van den Bos V., Wagner-Cremer F. 2022. Synchronous vegetation response to the last glacial-interglacial transition in northwest Europe, Communications Earth and Environment, 3, 1, -

Engels S., Medeiros A.S., Axford Y., Brooks S.J., Heiri O., Luoto T.P., Nazarova L., Porinchu D.F., Quinlan R., Self A.E. 2020. Temperature change as a driver of spatial patterns and long-term trends in chironomid (Insecta: Diptera) diversity, Global Change Biology, 26, 3, 1155-1169

Faegri K., Iversen J. 1975. Textbook of Pollen Analysis

Feurdean A., Perşoiu A., Tanţău I., Stevens T., Magyari E.K., Onac B.P., Marković S., Andrič M., Connor S., Fărcaş S., Gałka M., Gaudeny T., Hoek W., Kolaczek P., Kuneš P., Lamentowicz M., Marinova E., Michczyńska D.J., Perşoiu I., Płóciennik M., Słowiński M., Stancikaite M., Sumegi P., Svensson A., Tămaş T., Timar A., Tonkov S., Toth M., Veski S., Willis K.J., Zernitskaya V. 2014. Climate variability and associated vegetation response throughout Central and Eastern Europe (CEE) between 60 and 8ka, Quaternary Science Reviews, 106 206-224

Grimm E.C. 1991. [No title available], TILIA and TILIA.GRAPH , -

Hájková P., Pařil P., Petr L., Chattová B., Matys Grygar T., Heiri O. 2016. A first chironomid-based summer temperature reconstruction (13-5 ka BP) around 49°N in inland Europe compared with local lake development, Quaternary Science Reviews, 141 94-111

Halffman R., Lembrechts J., Radujković D., De Gruyter J., Nijs I., De Jonge C. 2022. Soil chemistry, temperature and bacterial community composition drive brGDGT distributions along a subarctic elevation gradient, Organic Geochemistry, 163 -

Harvey H.R., Fallon R.D., Patton J.S. 1986. The effect of organic matter and oxygen on the degradation of bacterial membrane lipids in marine sediments, Geochimica et Cosmochimica Acta, 50, 5, 795-804

Heiri O., Brooks S.J., Renssen H., Bedford A., Hazekamp M., Ilyashuk B., Jeffers E.S., Lang B., Kirilova E., Kuiper S., Millet L., Samartin S., Toth M., Verbruggen F., Watson J.E., Van Asch N., Lammertsma E., Amon L., Birks H.H., Birks H.J.B., Mortensen M.F., Hoek W.Z., Magyari E., Munõz Sobrino C., Seppä H., Tinner W., Tonkov S., Veski S., Lotter A.F. 2014. Validation of climate model-inferred regional temperature change for late-glacial Europe, Nature Communications, 5 -

Heiri O., Brooks S.J., Birks H.J.B., Lotter A.F. 2011. A 274-lake calibration data-set and inference model for chironomid-based summer air temperature reconstruction in Europe, Quaternary Science Reviews, 30, 23-24, 3445-3456

Heiri O., Lotter A.F. 2010. How does taxonomic resolution affect chironomid-based temperature reconstruction?, Journal of Paleolimnology, 44, 2, 589-601

Heiri O., Lotter A.F. 2005. Holocene and Lateglacial summer temperature reconstruction in the Swiss Alps based on fossil assemblages of aquatic organisms: A review, Boreas, 34, 4, 506-516

Heiri O., Lotter A.F. 2001. Effect of low count sums on quantitative environmental reconstructions: An example using subfossil chironomids, Journal of Paleolimnology, 26, 3, 343-350

Herber J., Klotz F., Frommeyer B., Weis S., Straile D., Kolar A., Sikorski J., Egert M., Dannenmann M., Pester M. 2020. A single Thaumarchaeon drives nitrification in deep oligotrophic Lake Constance, Environmental Microbiology, 22, 1, 212-228

Hopmans E.C., Schouten S., Sinninghe Damsté J.S. 2016. The effect of improved chromatography on GDGT-based palaeoproxies, Organic Geochemistry, 93 1-6

Hopmans E.C., Weijers J.W.H., Schefuß E., Herfort L., Sinninghe Damsté J.S., Schouten S. 2004. A novel proxy for terrestrial organic matter in sediments based on branched and isoprenoid tetraether lipids, Earth and Planetary Science Letters, 224, 45323, 107-116

Hošek J., Pokorný P., Prach J., Lisá L., Grygar T.M., Knésl I., Trubač J. 2017. Late Glacial erosion and pedogenesis dynamics: Evidence from high-resolution lacustrine archives and paleosols in south Bohemia (Czech Republic), Catena, 150 261-278

Huguet C., Schimmelmann A., Thunell R., Lourens L.J., Damsté J.S.S., Schouten S. 2007. A study of the TEX86 paleothermometer in the water column and sediments of the Santa Barbara Basin, California, Paleoceanography, 22, 3, -

Inglis G.N., Tierney J.E. 2020. The TEX86 Paleotemperature Proxy, The TEX86 Paleotemperature Proxy

Jankovská V. 2006. Late Glacial and Holocene history of Plešné Lake and its surrounding landscape based on pollen and palaeoalgological analyses, Biologia (Poland), 61, 20, -

Janský B., Šobr M., Kocum J., Česák J. 2005. New bathymetric mapping of the Bohemian Forest glacial lakes [Nová batymetrická mapování glaciálních jezer na české straně šumavy], Geografie-Sbornik CGS, 110, 3, 176-187

Juggins S. 2003. C User Guide. Software for Ecological and Palaeoecological Data Analysis and Visualisation2

Karger D.N., Nobis M.P., Normand S., Graham C.H., Zimmermann N.E. 2023. CHELSA-TraCE21k - high-resolution (1km) downscaled transient temperature and precipitation data since the Last Glacial Maximum, Climate of the Past, 19, 2, 439-456

Kim J.-H., Schouten S., Hopmans E.C., Donner B., Sinninghe Damsté J.S. 2008. Global sediment core-top calibration of the TEX86 paleothermometer in the ocean, Geochimica et Cosmochimica Acta, 72, 4, 1154-1173

Kopáček J., Hejzlar J., Krám P., Oulehle F., Posch M. 2016. Effect of industrial dust on precipitation chemistry in the Czech Republic (Central Europe) from 1850 to 2013, Water Research, 103 30-37

Kopácek J., Hejzlar J., Kana J., Porcal P., Pšenáková P., Vrba J. 2001. Element budgets in three Bohemian Forest lakes and their watersheds in the 2000 hydrological year: 11. Cerné Lake, Silva Gabreta, 6 53-72

Kotrys B., Płóciennik M., Sydor P., Brooks S.J. 2020. Expanding the Swiss-Norwegian chironomid training set with Polish data, Boreas, 49, 1, 89-107

Kubovčík V., Hošek J., Heiri O., Rojik F., Vaterková S., Trubač J., Pokorný P. 2021. Chironomid-based temperature and environmental reconstructions of the Last Glacial Termination in southern Bohemia, Czech Republic, Palaeogeography, Palaeoclimatology, Palaeoecology, 567 -

Kuneš P., Pelánková B., Chytrý M., Jankovská V., Pokorný P., Petr L. 2008. Interpretation of the last-glacial vegetation of eastern-central Europe using modern analogues from southern Siberia, Journal of Biogeography, 35, 12, 2223-2236

Liaw A., Wiener M. 2002. Classification and regression by randomForest, R News, 2, 3, 18-22

Lowe J.J., Rasmussen S.O., Björck S., Hoek W.Z., Steffensen J.P., Walker M.J.C., Yu Z.C. 2008. Synchronisation of palaeoenvironmental events in the North Atlantic region during the Last Termination: a revised protocol recommended by the INTIMATE group, Quaternary Science Reviews, 27, 45323, 6-17

Luoto T.P., Ojala A.E.K. 2017. Meteorological validation of chironomids as a paleotemperature proxy using varved lake sediments, Holocene, 27, 6, 870-878

Maraun D. 2016. Bias Correcting Climate Change Simulations - a Critical Review, Current Climate Change Reports, 2, 4, 211-220

Martin C., Ménot G., Thouveny N., Peyron O., Andrieu-Ponel V., Montade V., Davtian N., Reille M., Bard E. 2020. Early Holocene Thermal Maximum recorded by branched tetraethers and pollen in Western Europe (Massif Central, France), Quaternary Science Reviews, 228 -

Martin C., Ménot G., Thouveny N., Davtian N., Andrieu-Ponel V., Reille M., Bard E. 2019. Impact of human activities and vegetation changes on the tetraether sources in Lake St Front (Massif Central, France), Organic Geochemistry, 135 38-52

Mayewski P.A., Rohling E.E., Stager J.C., Karlén W., Maasch K.A., Meeker L.D., Meyerson E.A., Gasse F., van Kreveld S., Holmgren K., Lee-Thorp J., Rosqvist G., Rack F., Staubwasser M., Schneider R.R., Steig E.J. 2004. Holocene climate variability, Quaternary Research, 62, 3, 243-255

Mentlík P., Engel Z., Braucher R., Léanni L., Arnold M., Aumaître G., Bourlés D., Keddadouche K. 2013. Chronology of the Late Weichselian glaciation in the Bohemian Forest in Central Europe, Quaternary Science Reviews, 65 120-128

Meyers P.A., Lallier-Vergès E. 1999. Lacustrine sedimentary organic matter records of Late Quaternary paleoclimates, Journal of Paleolimnology, 21, 3, 345-372

Meyers P.A. 1994. Preservation of elemental and isotopic source identification of sedimentary organic matter, Chemical Geology, 114, 45385, 289-302

Moreno A., Svensson A., Brooks S.J., Connor S., Engels S., Fletcher W., Genty D., Heiri O., Labuhn I., Perşoiu A., Peyron O., Sadori L., Valero-Garcés B., Wulf S., Zanchetta G., Allen J.R.M., Ampel L., Blamart D., Birks H., Blockley S., Borsato A., Bos H., Brauer A., Combourieu-Nebout N., de Beaulieu J.-L., Drescher-Schneider R., Drysdale R., Elias S., Frisia S., Hellstrom J.C., Ilyashuk B., Joannin S., Kühl N., Larocque-Tobler I., Lotter A., Magny M., Matthews I., McDermott F., Millet L., Morellón M., Neugebauer I., Muñoz-Sobrino C., Naughton F., Ohlwein C., Roucoux K., Samartin S., Sánchez-Goñi M.-F., Sirocko F., van Asch N., van Geel B., van Grafenstein U., Vannière B., Vegas J., Veres D., Walker M., Wohlfarth B., Data contributors 2014. A compilation of Western European terrestrial records 60-8kaBP: Towards an understanding of latitudinal climatic gradients, Quaternary Science Reviews, 106 167-185

Moser K.A., Baron J.S., Brahney J., Oleksy I.A., Saros J.E., Hundey E.J., Sadro S.A., Kopáček J., Sommaruga R., Kainz M.J., Strecker A.L., Chandra S., Walters D.M., Preston D.L., Michelutti N., Lepori F., Spaulding S.A., Christianson K.R., Melack J.M., Smol J.P. 2019. Mountain lakes: Eyes on global environmental change, Global and Planetary Change, 178 77-95

Müller D., Tjallingii R., Płóciennik M., Luoto T.P., Kotrys B., Plessen B., Ramisch A., Schwab M.J., Błaszkiewicz M., Słowiński M., Brauer A. 2021. New insights into lake responses to rapid climate change: the Younger Dryas in Lake Gościąż, central Poland, Boreas, 50, 2, 535-555

Oksanen J., Blanchet F.G., Kindt R., Legendre P., Minchin P.R., O'Hara R.B., Simpson G.L., Solymos P., Stevens M.H.H., Wagner H. 2012. Vegan: Community ecology package, R package version, 2 -

Ortu E., Brewer S., Peyron O. 2006. Pollen-inferred palaeoclimate reconstructions in mountain areas: Problems and perspectives, Journal of Quaternary Science, 21, 6, 615-627

Peinerud E.K. 2000. Interpretation of Si concentrations in lake sediments: Three case studies, Environmental Geology, 40, 45323, 64-72

Peterse F., van der Meer J., Schouten S., Weijers J.W.H., Fierer N., Jackson R.B., Kim J.-H., Sinninghe Damsté J.S. 2012. Revised calibration of the MBT-CBT paleotemperature proxy based on branched tetraether membrane lipids in surface soils, Geochimica et Cosmochimica Acta, 96 215-229

Płóciennik M., Self A., Birks H.J.B., Brooks S.J. 2011. Chironomidae (Insecta: Diptera) succession in Zabieniec bog and its palaeo-lake (central Poland) through the Late Weichselian and Holocene, Palaeogeography, Palaeoclimatology, Palaeoecology, 307, 45383, 150-167

Pokorný P. 2002. A high-resolution record of Late-Glacial and Early-Holocene climatic and environmental change in Czech Republic, Quaternary International, 91, 1, 101-122

Powers L., Werne J.P., Vanderwoude A.J., Sinninghe Damsté J.S., Hopmans E.C., Schouten S. 2010. Applicability and calibration of the TEX86 paleothermometer in lakes, Organic Geochemistry, 41, 4, 404-413

PražÁkqyá M., Fott J., Veselý J., Majer V., KopáČek J. 2006. The long-term succession of cladoceran fauna and palaeoclimate forcing: A 14,600Ùyear record from Plešné Lake, the Bohemian Forest, Biologia (Poland), 61, 20, -

Punt W., Clarke G.C.S. 2004. [No title available], The Northwest European Pollen Flora , -

Ramos-Román M.J., De Jonge C., Magyari E., Veres D., Ilvonen L., Develle A.-L., Seppä H. 2022. Lipid biomarker (brGDGT)- and pollen-based reconstruction of temperature change during the Middle to Late Holocene transition in the Carpathians, Global and Planetary Change, 215 -

Rasmussen S.O., Bigler M., Blockley S.P., Blunier T., Buchardt S.L., Clausen H.B., Cvijanovic I., Dahl-Jensen D., Johnsen S.J., Fischer H., Gkinis V., Guillevic M., Hoek W.Z., Lowe J.J., Pedro J.B., Popp T., Seierstad I.K., Steffensen J.P., Svensson A.M., Vallelonga P., Vinther B.M., Walker M.J.C., Wheatley J.J., Winstrup M. 2014. A stratigraphic framework for abrupt climatic changes during the Last Glacial period based on three synchronized Greenland ice-core records: Refining and extending the INTIMATE event stratigraphy, Quaternary Science Reviews, 106 14-28

Rasmussen S.O., Andersen K.K., Svensson A.M., Steffensen J.P., Vinther B.M., Clausen H.B., Siggaard-Andersen M.-L., Johnsen S.J., Larsen L.B., Dahl-Jensen D., Bigler M., Röthlisberger R., Fischer H., Goto-Azuma K., Hansson M.E., Ruth U. 2006. A new Greenland ice core chronology for the last glacial termination, Journal of Geophysical Research Atmospheres, 111, 6, -

Rehfeld K., Trachsel M., Telford R.J., Laepple T. 2016. Assessing performance and seasonal bias of pollen-based climate reconstructions in a perfect model world, Climate of the Past, 12, 12, 2255-2270

Reimer P.J., Austin W.E.N., Bard E., Bayliss A., Blackwell P.G., Bronk Ramsey C., Butzin M., Cheng H., Edwards R.L., Friedrich M., Grootes P.M., Guilderson T.P., Hajdas I., Heaton T.J., Hogg A.G., Hughen K.A., Kromer B., Manning S.W., Muscheler R., Palmer J.G., Pearson C., Van Der Plicht J., Reimer R.W., Richards D.A., Scott E.M., Southon J.R., Turney C.S.M., Wacker L., Adolphi F., Büntgen U., Capano M., Fahrni S.M., Fogtmann-Schulz A., Friedrich R., Köhler P., Kudsk S., Miyake F., Olsen J., Reinig F., Sakamoto M., Sookdeo A., Talamo S. 2020. The IntCal20 Northern Hemisphere Radiocarbon Age Calibration Curve (0-55 cal kBP), Radiocarbon, 62, 4, 725-757

Renssen H., Mairesse A., Goosse H., Mathiot P., Heiri O., Roche D.M., Nisancioglu K.H., Valdes P.J. 2015. Multiple causes of the Younger Dryas cold period, Nature Geoscience, 8, 12, 946-949

Renssen H., Isarin R.F.B. 2001. The two major warming phases of the last deglaciation at ∼14.7 and ∼11.5 ka cal BP in Europe: Climate reconstructions and AGCM experiments, Global and Planetary Change, 30, 45383, 117-153

Rieradevall M., Brooks S.J. 2001. An identification guide to subfossil Tanypodinae larvae (Insecta: Diptera: Chironomidae) based on cephalic setation, Journal of Paleolimnology, 25, 1, 81-99

Robles M., Peyron O., Ménot G., Brugiapaglia E., Wulf S., Appelt O., Blache M., Vannière B., Dugerdil L., Paura B., Ansanay-Alex S., Cromartie A., Charlet L., Guédron S., De Beaulieu J.-L., Joannin S. 2023. Climate changes during the Late Glacial in southern Europe: new insights based on pollen and brGDGTs of Lake Matese in Italy, Climate of the Past, 19, 2, 493-515

Schillereff D.N., Chiverrell R.C., Boyle J.F., Croudace I.W. 2015. An inter-comparison of µXRF scanning analytical methods, Developments in Palaeoenvironmental Research: Micro-XRF Studies of Sediment Cores , 110-120

Schouten S., Hopmans E.C., Sinninghe Damsté J.S. 2013. The organic geochemistry of glycerol dialkyl glycerol tetraether lipids: A review, Organic Geochemistry, 54 19-61

Schouten S., Hopmans E.C., Schefuß E., Sinninghe Damsté J.S. 2002. Distributional variations in marine crenarchaeotal membrane lipids: A new tool for reconstructing ancient sea water temperatures?, Earth and Planetary Science Letters, 204, 45323, 265-274

Schwark L., Zink K., Lechterbeck J. 2002. Reconstruction of postglacial to early Holocene vegetation history in terrestrial Central Europe via cuticular lipid biomarkers and pollen records from lake sediments, Geology, 30, 5, 463-466

Scordo F., Chandra S., Suenaga E., Kelson S.J., Culpepper J., Scaff L., Tromboni F., Caldwell T.J., Seitz C., Fiorenza J.E., Williamson C.E., Sadro S., Rose K.C., Poulson S.R. 2021. Smoke from regional wildfires alters lake ecology, Scientific Reports, 11, 1, -

Sinninghe Damsté J.S., Weber Y., Zopfi J., Lehmann M.F., Niemann H. 2022. Distributions and sources of isoprenoidal GDGTs in Lake Lugano and other central European (peri-)alpine lakes: Lessons for their use as paleotemperature proxies, Quaternary Science Reviews, 277 -

Sinninghe Damsté J.S., Ossebaar J., Schouten S., Verschuren D. 2012. Distribution of tetraether lipids in the 25-ka sedimentary record of Lake Challa: Extracting reliable TEX 86 and MBT/CBT palaeotemperatures from an equatorial African lake, Quaternary Science Reviews, 50 43-54

Stivrins N., Belle S., Trasune L., Blaus A., Salonen S. 2021. Food availability and temperature optima shaped functional composition of chironomid assemblages during the Late Glacial–Holocene transition in Northern Europe, Quaternary Science Reviews, 266 -

Stockmarr J. 1971. Tablets with spores used in absolute pollen analysis, Pollen et Spores, 13, 4, 615-621

Summons R.E., Jahnke L.L., Roksandic Z. 1994. Carbon isotopic fractionation in lipids from methanotrophic bacteria: Relevance for interpretation of the geochemical record of biomarkers, Geochimica et Cosmochimica Acta, 58, 13, 2853-2863

Svobodová H., Reille M., Goeury C. 2001. Past vegetation dynamics of Vltavský luh, upper Vltava river valley in the Šumava mountains, Czech Republic, Vegetation History and Archaeobotany, 10, 4, 185-199

TÁtosová J., Veselý J., Stuchlí E. 2006. Holocene subfossil chironomid stratigraphy (Diptera: Chironomidae) in the sediment of Plešné Lake (the Bohemian Forest, Czech Republic): Palaeoenvironmental implications, Biologia (Poland), 61, 20, -

ter Braak C.J.F., Juggins S. 1993. Weighted averaging partial least squares regression (WA-PLS): an improved method for reconstructing environmental variables from species assemblages, Hydrobiologia, 269-270, 1, 485-502

Teranes J.L., Bernasconi S.M. 2005. Factors controlling δ13C values of sedimentary carbon in hypertrophic Baldeggersee, Switzerland, and implications for interpreting isotope excursions in lake sedimentary records, Limnology and Oceanography, 50, 3, 914-922

Tollefsrud M.M., Kissling R., Gugerli F., Johnsen Ø., Skrøppa T., Cheddadi R., Van Der Knaap W.O., Latałowa M., Terhürne-Berson R., Litt T., Geburek T., Brochmann C., Sperisen C. 2008. Genetic consequences of glacial survival and postglacial colonization in Norway spruce: Combined analysis of mitochondrial DNA and fossil pollen, Molecular Ecology, 17, 18, 4134-4150

Tóth M., Magyari E.K., Brooks S.J., Braun M., Buczkó K., Bálint M., Heiri O. 2012. A chironomid-based reconstruction of late glacial summer temperatures in the southern Carpathians (Romania), Quaternary Research, 77, 1, 122-131

Turek J., Fluksová H., Hejzlar J., Kopáček J., Porcal P. 2014. Modelling air temperature in catchments of Čertovo and Plešné lakes in the Bohemian Forest back to 1781, Silva Gabreta, 20, 1, 1-24

Tyler J.J., Nederbragt A.J., Jones V.J., Thurow J.W. 2010. Assessing past temperature and soil pH estimates from bacterial tetraether membrane lipids: Evidence from the recent lake sediments of Lochnagar, Scotland, Journal of Geophysical Research: Biogeosciences, 115, 1, -

Veski S., Seppä H., Stančikaite M., Zernitskaya V., Reitalu T., Gryguc G., Heinsalu A., Stivrins N., Amon L., Vassiljev J., Heiri O. 2015. Quantitative summer and winter temperature reconstructions from pollen and chironomid data between 15 and 8 ka BP in the Baltic-Belarus area, Quaternary International, 388 4-11

Vočadlová K., Petr L., Žáčková P., Křížek M., Křížová L., Hutchinson S.M., Šobr M. 2015. The Lateglacial and Holocene in Central Europe: A multi-proxy environmental record from the Bohemian Forest, Czech Republic, Boreas, 44, 4, 769-784

Walker I.R., Smol J.P., Engstrom D.R., Birks H.J.B. 1991. An assessment of Chironomidae as quantitative indicators of past climatic change, Canadian Journal of Fisheries and Aquatic Sciences, 48, 6, 975-987

Watson B.I., Williams J.W., Russell J.M., Jackson S.T., Shane L., Lowell T.V. 2018. Temperature variations in the southern Great Lakes during the last deglaciation: Comparison between pollen and GDGT proxies, Quaternary Science Reviews, 182 78-92

Weijers J.W.H., Schouten S., van den Donker J.C., Hopmans E.C., Sinninghe Damsté J.S. 2007. Environmental controls on bacterial tetraether membrane lipid distribution in soils, Geochimica et Cosmochimica Acta, 71, 3, 703-713

Whiticar M.J. 1999. Carbon and hydrogen isotope systematics of bacterial formation and oxidation of methane, Chemical Geology, 161, 1, 291-314

Whitlock C., Larsen C. 2001. Charcoal as a fire proxy, Tracking Environmental Change Using Lake Sediments , 75-97

Wischnewski J., Mischke S., Wang Y., Herzschuh U. 2011. Reconstructing climate variability on the northeastern Tibetan Plateau since the last Lateglacial - a multi-proxy, dual-site approach comparing terrestrial and aquatic signals, Quaternary Science Reviews, 30, 45323, 82-97

Wohlfarth B., Luoto T.P., Muschitiello F., Väliranta M., Björck S., Davies S.M., Kylander M., Ljung K., Reimer P.J., Smittenberg R.H. 2018. Climate and environment in southwest Sweden 15.5–11.3 cal. ka BP, Boreas, 47, 3, 687-710

Wuchter C., Schouten S., Wakeham S.G., Sinninghe Damsté J.S. 2005. Temporal and spatial variation in tetraether membrane lipids of marine Crenarchaeota in particulate organic matter: Implications for TEX86 paleothermometry, Paleoceanography, 20, 3, 1-11

Xiao W., Wang Y., Zhou S., Hu L., Yang H., Xu Y. 2016. Ubiquitous production of branched glycerol dialkyl glycerol tetraethers (brGDGTs) in global marine environments: A new source indicator for brGDGTs, Biogeosciences, 13, 20, 5883-5894

R Core Team 2022. R: A Language and Environment for Statistical Computing, R: A Language and Environment for Statistical Computing,